Query Details

1. Please check if the affiliations are presented correctly.

2. Please check if the section headings are assigned to appropriate levels.

Original Article

Reversal of biological age in multiple rat organs by young porcine plasma fraction

Steve Horvath ✉
Email : shorvath@mednet.ucla.edu
Affiliationids : Aff1 Aff2 Aff3, Correspondingaffiliationid : Aff3

Kavita Singh   Affiliationids : Aff4

Ken Raj   Affiliationids : Aff3

Shraddha Khairnar   Affiliationids : Aff4

Akshay Sanghavi   Affiliationids : Aff5

Agnivesh Shrivastava   Affiliationids : Aff5

Joseph A. Zoller   Affiliationids : Aff2

Caesar Z. Li   Affiliationids : Aff2

Claudia B. Herenu   Affiliationids : Aff6

Martina Canatelli-Mallat   Affiliationids : Aff7

Marianne Lehmann   Affiliationids : Aff7

Siniša Habazin   Affiliationids : Aff8

Mislav Novokmet   Affiliationids : Aff8

Frano Vučković   Affiliationids : Aff8

Leah C. Solberg Woods   Affiliationids : Aff9

Angel Garcia Martinez   Affiliationids : Aff10

Tengfei Wang   Affiliationids : Aff10

Priscila Chiavellini   Affiliationids : Aff7

Andrew J. Levine   Affiliationids : Aff11

Hao Chen   Affiliationids : Aff10

Robert T. Brooke   Affiliationids : Aff12

Juozas Gordevicius   Affiliationids : Aff12

Gordan Lauc   Affiliationids : Aff8 Aff13

Rodolfo G. Goya   Affiliationids : Aff7

Harold L. Katcher ✉
Email : har.kat@yuvanresearch.com
Affiliationids : Aff5, Correspondingaffiliationid : Aff5

Aff1 Department of Human Genetics, David Geffen School of Medicine, University of California, Los Angeles, CA, USA

Aff2 Department of Biostatistics, Fielding School of Public Health, University of California, Los Angeles, CA, USA

Aff3 Altos Labs, Cambridge, UK

Aff4 Shobhaben Pratapbhai Patel School of Pharmacy and Technology Management, SVKM's NMIMS University, Mumbai, India

Aff5 Yuvan Research Inc., Mountain View, CA, USA

Aff6 Institute for Experimental Pharmacology of Cordoba (IFEC), School of Chemical Sciences, National University of Cordoba, Cordoba, Argentina

Aff7 Biochemistry Research Institute of La Plata–Histology B, Pathology B, School of Medicine, University of La Plata, La Plata, Argentina

Aff8 Genos Glycoscience Research Laboratory, Zagreb, Croatia

Aff9 Wake Forest University School of Medicine, Medical Center Drive, Winston Salem, NC, USA

Aff10 Department of Pharmacology, Addiction Science and Toxicology, The University of Tennessee Health Science Center, Memphis, TN, USA

Aff11 Department of Neurology, David Geffen School of Medicine at the University of California, Los Angeles, CA, USA

Aff12 Epigenetic Clock Development Foundation, Torrance, CA, USA

Aff13 Faculty of Pharmacy and Biochemistry, University of Zagreb, Zagreb, Croatia

Abstract

Young bl AQ1 ood plasma is known to confer beneficial effects on various organs in mice and rats. However, it was not known whether plasma from young adult pigs rejuvenates old rat tissues at the epigenetic level; whether it alters the epigenetic clock, which is a highly accurate molecular biomarker of aging. To address this question, we developed and validated six different epigenetic clocks for rat tissues that are based on DNA methylation values derived from $n = 613$ tissue samples. As indicated by their respective names, the rat pan-tissue clock can be applied to DNA methylation profiles from all rat tissues, while the rat brain, liver, and blood clocks apply to the corresponding tissue types. We also developed two epigenetic clocks that apply to both human and rat tissues by adding $n = 1366$ human tissue samples to the training data. We employed these six rat clocks to investigate the rejuvenation effects of a porcine plasma fraction treatment in different rat tissues. The treatment more than halved the epigenetic ages of blood, heart, and liver tissue. A less pronounced, but statistically significant, rejuvenation effect could be observed in the hypothalamus. The treatment was accompanied by progressive improvement in the function of these organs as ascertained through numerous biochemical/physiological biomarkers, behavioral responses encompassing cognitive functions. An immunoglobulin G (IgG) N-glycosylation pattern shift from pro- to anti-inflammatory also indicated reversal of glycan aging. Overall, this study demonstrates that a young porcine plasma-derived treatment markedly reverses aging in rats according to epigenetic clocks, IgG glycans, and other biomarkers of aging.

Keywords

Rejuvenation
Plasma fraction
Epigenetic clock
DNA methylation
Glycans
Rat

Steve Horvath, Kavita Singh, and Ken Raj share joint first authorship.

Supplementary Information

The online version contains supplementary material available at https://doi.org/10.1007/s11357-023-00980-6.

Introdu AQ2 ction

The field of heterochronic parabiosis, involving the mixing of blood from young and old mice, laid the groundwork for investigations into the impacts of exposing an aged organism to a youthful systemic environment. Originating in rats before expanding to mice, this field was initially pioneered by Clive McCay who employed it in the study of aging in rats, although early attempts were hampered by the widespread occurrence of "parabiotic disease" [1, 2]. Progressing through time, surgical methods improved, and rat studies by Ludwig and Elashoff [3] unveiled the lifespan extension of an older parabiont when partnered with a younger one, presenting the first evidence of extended life in the older organism as a response to a youthful environment.

Later investigations using mice revealed insights into aging physiology and stem cell behavior across different tissues and organ systems [4, 5]. Beneficial influences of young blood on various murine organs were evident in functional tests, with outcomes suggesting that the beneficial effects were a result of blood-borne factors as opposed to indirect benefits from the young mice's superior organ functionality [6, 7, 8, 9, 10, 11, 12]. The ensuing interest led to widespread research and commercial attention on the identification and isolation of rejuvenation factors from blood that could potentially mitigate or treat age-related conditions.

However, in the context of aging and rejuvenation, it is crucial to differentiate between improved health or organ function, which could be achieved via medication or surgery, and genuine molecular age reversal. Clinical biomarkers, despite their utility in indicating organ dysfunction or disease, fall short of accurately indicating fundamental aging mechanisms [13]. With this in mind, our study tackles the question of whether plasma fraction treatment or similar interventions can truly reverse biological age, using two molecular aging biomarkers — DNA methylation and glycosylation.

Epigenetic changes, including cytosine methylation, are a well-established hallmark of aging, useful for developing accurate age estimators [14, 15, 16, 17, 18, 19, 20, 21]. Notably, DNA methylation (DNAm) age estimators apply broadly, including to sorted cells, tissues, and organs, across the entire age spectrum. The difference between DNAm age and chronological age, termed "epigenetic age acceleration," is predictive of all-cause mortality and is associated with a wide variety of conditions [22, 23, 24, 25, 26, 27, 28, 29, 30].

Epigenetic clocks have been successfully used to evaluate age-related interventions in mice [31, 32, 33, 34, 35]. Here we present six epigenetic clocks for rats, two of which are applicable to humans as well.

Complementing the epigenetic clocks, analyses of human immunoglobulin G (IgG) have established that changes in its N-glycome composition occur with aging and disease, providing a "glycan clock" that can indicate age and be reversed through lifestyle changes [36, 37].

This paper aims to address the question: will young plasma from pigs reverse the biological age of rat tissues? To assess this, we used these six rat-specific epigenetic clocks along with IgG N-glycan profiling, physiological, histological, biochemical, and cognitive assessments, to evaluate the plasma fraction-based treatment in tissues from 2-year-old rats. Our findings demonstrate that this approach greatly reverses aging in rats.

Results

DNA methylation data

All DNA methylation data were generated on a custom methylation array that applies to all mammals. We obtained in total, DNA methylation profiles of $n = 613$ samples from 13 different tissues of rat (*Rattus norvegicus*) (Supplementary Table S1 , Supplementary Table S2 , Supplementary Table S3), with ages that ranged from 0.0384 years (i.e., 2 weeks) to 2.3 years (i.e., 120 weeks). Our study utilized large sample sizes and multiple trials carried out by labs with different scientific backgrounds (Supplementary Figure 1): (i) India (Yuvan Research in collaboration with NMIMS School of Pharmacy's), (ii) the USA (H. Chen and L. Solberg Woods), and (iii) Argentina (R. Goya). Unsupervised hierarchical clustering shows that the methylation profiles clustered by tissue type, as would be expected (Supplementary Fig. 2).

Our DNA methylation-based age estimators (epigenetic clocks) were developed ("trained" in the parlance of machine learning) using $n = 503$ rat tissues. The two epigenetic clocks that apply to both species were developed by adding $n = 1366$ human tissue samples to the rat training set. Both rat and human tissues were profiled on the same methylation array platform (HorvathMammalMethylChip40) that includes 36,000 highly conserved CpGs [38] (" Methods ").

Epigenetic clocks

Our six different clocks for rats can be distinguished along several dimensions (tissue type, species, and measure of age). Some clocks apply to all tissues (pan-tissue clocks) while others are tailor-made for specific tissues/organs (brain, blood, liver). The rat pan-tissue clock was trained on all available tissues. The brain clock was trained using DNA samples extracted from whole brain, hippocampus, hypothalamus, neocortex, substantia nigra, cerebellum, and the pituitary gland. The liver and blood clocks were trained using the liver and blood samples from the training set, respectively. While the four rat clocks (pan-tissue, brain, blood, and liver clocks) apply only to rats, the human-rat clocks apply to both species. The two human-rat pan-tissue clocks are distinct, by way of measurement parameters. One estimates *absolute* age (in units of years), while the other estimates *relative* age, which is the ratio of chronological age to maximum lifespan, with values between 0 and 1. This ratio allows alignment and biologically meaningful comparison between species with very different lifespans (rat and human), which is not afforded by mere measurement of absolute age.

To arrive at unbiased estimates of the six epigenetic clocks, we used (a) cross-validation of the training data and (b) evaluation with an independent test data set. The cross-validation study reports unbiased estimates of the age correlation R (defined as Pearson correlation between the age estimate (DNAm age) and chronological age) as well as the median absolute error (Fig. 1). The cross-validation estimates of the age correlations for all six clocks are higher than 0.85. The four rat clocks exhibited absolute errors that range from 0.137 years (1.6 months) for the rat blood clock to 0.182 years (2.2 months) for the rat pan-tissue clock (Fig. 1 A–D). The human-rat clock for age generated an age correlation of $R = 0.99$ when both species are analyzed together (Fig. 1 E) but is lower when the analysis is restricted to rat tissues alone ($R = 0.85$, Fig. 1 F). In contrast, the human-rat clock for *relative age* exhibits high correlation regardless of whether the analysis is done with samples from both species ($R = 0.96$, Fig. 1 G) or only with rat samples ($R = 0.94$, Fig. 1 H). This demonstrates that relative age circumvents the skewing that is inherent when absolute age of species with very different lifespans are measured using a single formula. This is due in part to the unequal distribution of training data at the opposite ends of the age range.

Fig. 1

Cross-validation study of six epigenetic clocks for rat. **A–D** Four epigenetic clocks that were trained on rat tissues only. All estimates of epigenetic age and their matching chronological ages are measured in years. **E–H** Results for two clocks that were trained on both human and rat tissues. Leave-one-sample-out estimate of DNA methylation age (*y*-axis, in units of years) versus chronological age for **A** rat pan-tissue, **B**

rat brain, **C** rat blood, and **D** rat liver clock. Dots are colored by **A** tissue type or **B** brain region. **E** and **F** "Human-rat" clock estimate of absolute age. **G**, **H** Human-rat clock estimate of relative age, which is the ratio of chronological age to the maximum lifespan of the respective species. Tenfold cross-validation estimates of age (*y*-axis, in years) in **E**, **G** human (green) and rat (orange) samples and **F**, **H** rat samples only (colored by tissue type). Each panel reports the sample size, correlation coefficient, median absolute error (MAE)
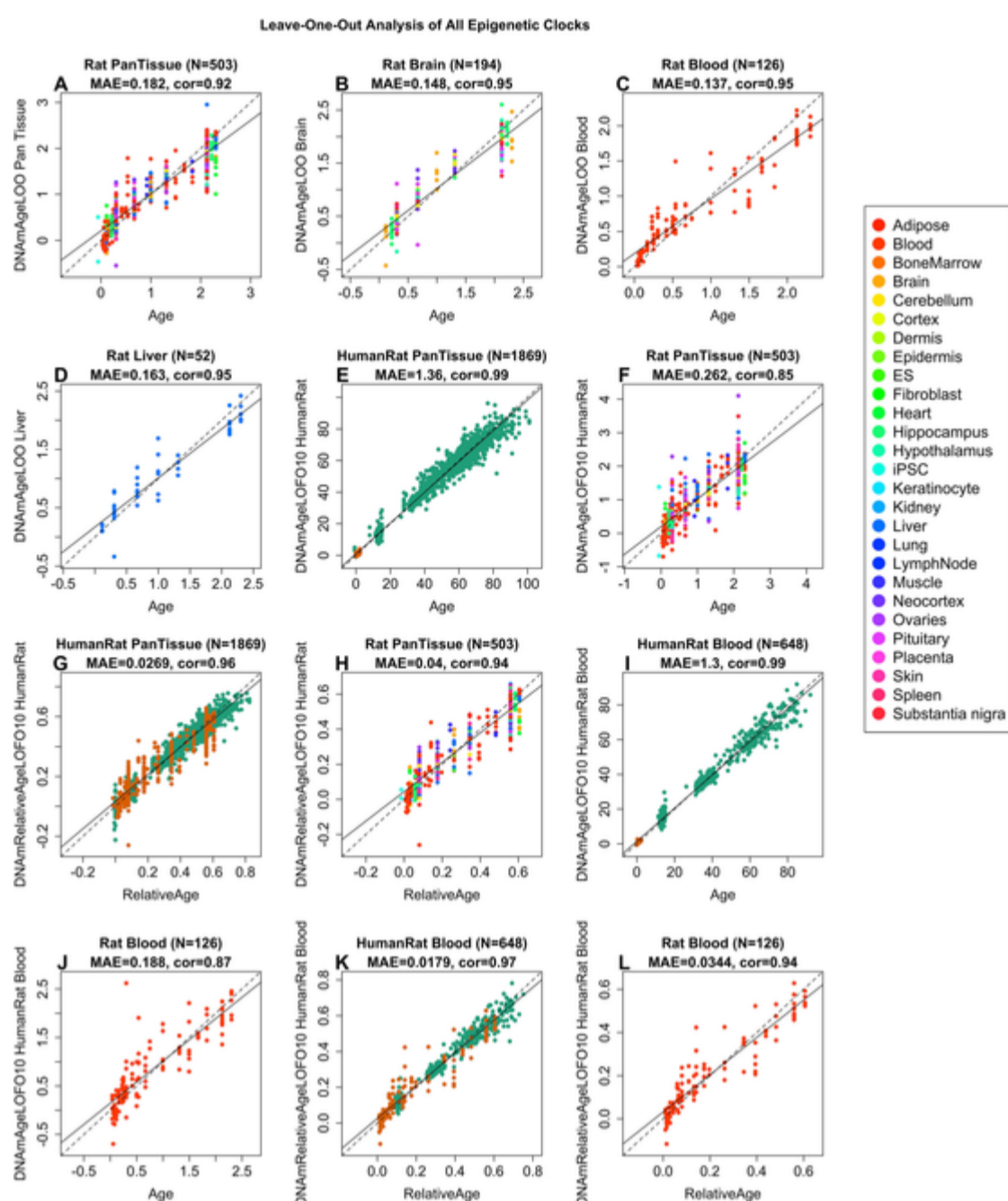
As indicated by its name, the rat pan-tissue clock is highly accurate in age estimation of all the different tissue samples tested and its performance with individual tissues can be more clearly seen in Supplementary Fig. 3. We also evaluated the accuracy of the six epigenetic clocks in independent test data from the plasma fraction test study. In the untreated rat tissue samples, the epigenetic clocks exhibited high age correlations in all tissues ($R \geq 0.95$ in blood, liver, and the hypothalamus and $R \geq 0.89$ in heart tissue, Supplementary Fig. 4).

Rejuvenation effect of the plasma fraction treatment

The ability to generate epigenetic age clocks for specific rat organs can be readily appreciated from the perspective of their practical utility in aging research. However, the appreciation of a pan-tissue clock is much deeper as it extends into the conceptual aspect with regard to aging. The ability to estimate the age of different rat organs with a single clock, be it the rat pan-tissue clock or the human-rat pan-tissue clock, is a very strong indicator that epigenetic age is regulated across all tissues of an organism, and this regulation is mediated systemically. This in turn implies that it may be possible to alter the rate of aging centrally and simultaneously across different tissues of the body, a principle that underlies the plasma fraction treatment.

The plasma fraction treatment E5 used in the investigation ("Methods") is based on the principle of heterochronic plasma exchange (HPE) [39], which does not involve the physical attachment of the circulatory systems of two animals. In addition to greatly reducing the stress to the animals, this is expected to have a more profound effect as 100% of the old animal's blood could in theory be replaced. This contrasts with heterochronic parabiosis, where a young rat, with approximately half the weight of an old rat, contributes less than 50% of the combined plasma circulation in the parabiotic partners. The general loss of tissue repair with age may reflect the negative influence of age-accumulated inhibitory proteins in aged tissues and circulation [40]. Therefore, if putative pro-aging factors are present in the plasma of old animals [40], they would be present in the old parabiotic partner and be distributed to the young one, causing it to age more rapidly. The plasma fraction treatment described here is a step change from HPE, as it uses neither whole blood nor plasma, but the exosome fraction of the plasma, which we term as E5. Another significant novelty is the source of E5, which were young adult pigs. The significance and implications of this are elaborated in the "Discussion" section below.

We evaluated the E5 treatment in several different rat studies (Supplementary Fig. 1). First, we applied the six clocks to an independent test data set (*n* = 76) comprising four rat tissues (blood, liver, heart, hypothalamus) to test whether a porcine plasma fraction from 6-month-old young adult pigs, injected into 2-year-old male rats, would reverse their epigenetic age. Plasma fraction treatment was administered to male rats following the experimental plan depicted in Supplementary Fig. 5. Briefly, 18 male Sprague-Dawley rats were divided into three groups: a group of six young rats (30 weeks old), a second group of six old rats (109 weeks old), and a third group of six plasma fraction-treated old rats (also 109 weeks old). Plasma fraction treatment consists of two series of intravenous injections of E5.

Rats were injected four times on alternate days for 8 days. A second identical series of injections were administered 95 days later. In its entirety, the experiment lasted 155 days. For the duration of the experiment, blood was drawn at regular intervals for hematological and biochemical analyses to monitor the impact of the treatment on blood, and solid vital organs. Cognitive functions of the rats were assessed four times during this period and at the end of the experiment, the animals were sacrificed, and DNA methylation profiles of several organs were generated. The DNA methylation profiles were evaluated using the above-mentioned six epigenetic clocks. The results derived from these profiles are plotted in Fig. 2, which shows that the epigenetic ages of the old and young rats are readily distinguishable by all the six clocks. Crucially, plasma treatment of the old rats reduced the epigenetic ages of blood, liver, and heart by a very large and significant margin, to levels that are comparable with those of the young rats. According to the six epigenetic clocks, the plasma fraction treatment rejuvenated liver by 74.6% (ranging from 68.6 to 78.6% depending on the clock, Supplementary Table S4), blood by 64.3% (ranging from 52.5 to 74.5%), heart by 46.5%, and hypothalamus by 24.4%. It is necessary to point out that the epigenetic clocks that were employed to analyze these experimental samples were developed independently of any of the methylation data from the experimental samples. This is important as it establishes that the E5-induced rejuvenation that was observed were not influenced by the way these clocks were developed. After having convincingly demonstrated that, we included DNA methylation profiles from the untreated controls of the experiment to the training set, to derive an even more accurate clock (elaborated in the section below). Epigenetic age measurements of the experimental samples with the resulting epigenetic clocks show rejuvenation effects of E5 that are even more pronounced: liver 77.6%, blood 68.2%, heart 56.5%, hypothalamus 29.6%, with the average rejuvenation across four tissues of 67.40%. In other words, the treatment more than halved the epigenetic age (Fig. 2 I–P).

Fig. 2

Epigenetic clock analysis of plasma fraction treatment. Six epigenetic clocks applied to independent test data from four rat tissue type (columns): blood, liver, heart, and hypothalamus. **A–D** Rat pan-tissue clock. **E** Rat blood clock applied to blood. **F** Rat liver clock applied to liver. **G** Rat blood clock applied to heart. **H** Rat brain clock applied to hypothalamus. **I–L** Human-rat clock measure of absolute age. **M–P** Human-rat clock measure of relative age defined as age/maximum species lifespan. Each bar plot reports the mean value and one standard error. *p* values result from analysis of variance. Student's *T* test *p* values result from a two-group comparison of old controls (left bar) versus old, treated samples (right bar), i.e., the young controls were omitted
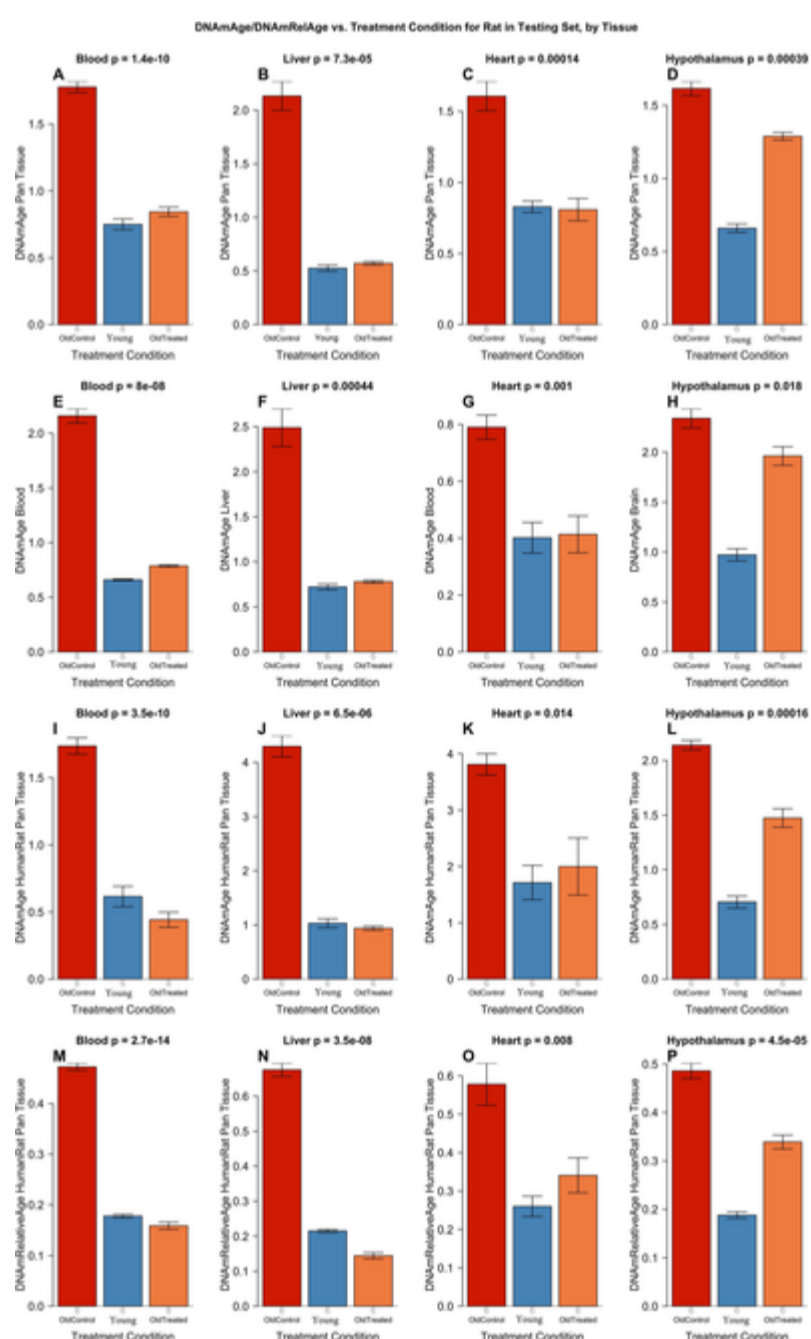
Final version of epigenetic clocks

These final versions of clocks were developed by adding the "untreated" samples from the E5 test data to the original training data ($n = 503$ rat tissues). This increased sample size of the training data led to clocks with higher accuracy, as shown by a cross-validation analysis (Supplementary Fig. 6, Supplementary Fig. 7). Using this final version of the epigenetic clocks, we find that the treatment effects were even more significant especially for the hypothalamus (Supplementary Fig. 8). Final versions of the pan-tissue clock, liver clock, blood clock, brain clock, and "human-rat" clock can be found in Supplementary Material. These clocks are recommended for use in future experiments with rats.

EWAS of age and treatment effects

Epigenetic clocks are attractive aggregate biomarkers because they summarize the information of many CpGs into a single number (the age estimate). They are nevertheless products of only a subset of age-related CpG changes. Hence, it is also informative to look at all CpGs in response to treatment. We executed an epigenome-wide association study, employing a false discovery rate threshold of 0.05 for both aging and treatment effects (refer to " Methods " for details). A strong reversal in age-related methylation gain post-E5 treatment was observed in blood, liver, heart, and the hypothalamus, as presented in Supplementary Fig. 9 . In summary, E5 treatment effectively reversed the alterations in methylation at individual CpGs, which typically occur with aging.

Physical and overt effects

The reduction of epigenetic age of E5-treated rats is particularly significant as it would appear to indicate that aging is a coordinated process as opposed to a stochastic one that occurs independently between the different organs. Before any further consideration of this notion, it is necessary to determine whether the reduction in epigenetic age is indeed biologically meaningful. In other words, is the rejuvenation of epigenetic age accompanied by changes in other well-characterized age-related endpoints. Equally important is the need to determine whether E5 treatment generated any adverse side effects.

The weight of rats for the duration of the experiment was monitored at regular intervals and the plots in Supplementary Fig. 10 A indicate that E5 treatment did not affect food intake and appetite in any way, as the weight of the treated and untreated rats were similar, and there was no presentation of any overt signs of physical or behavioral abnormality. These features replicated those we observed in a mid-term (30-day) pilot experiment, where in addition, we also measured and found grip strength of old rats to be considerably improved by this treatment (Supplementary Fig. 10 B, Supplementary Table S5). At 15 days post-treatment, the strength of plasma fraction-treated old rats was indistinguishable from that of young ones. These and other encouraging results from the mid-term pilot study prompted a longer-term (155-day) investigation, with a new preparation of E5. The result from this study forms the main corpus of this report. These two independent investigations produced similar results that varied only in terms of magnitude, as is consistent with their different durations. Histological examinations of the various organs did not indicate any obvious abnormalities after 155 days of treatment (Supplementary Fig. 11 and Supplementary Table S6). Instead, oil red O staining showed that accumulation of fat in old tissues was greatly reduced in E5-treated rats (Supplementary Fig. 12).

Blood cell indices and hematology

To monitor potential effects of E5 on the blood of rats, we measured hemoglobin levels, mean corpuscular volume (MCV), mean corpuscular hemoglobin (MCH), mean corpuscular hemoglobin concentration (MCHC), and hematocrit (HCT) levels and obtained counts of red blood cells, platelets, white blood cells, and lymphocytes at 0, 60, and 155 days from the start of treatment. These blood indices are informative indicators of malfunction of bone marrow and vital organs and importantly, they vary with the age of the animal. In all these, blood indices were very different between young and old rats at the start of the experiment, and in time, plasma fraction treatment nudged all these parameters, except for platelets, away from the values exhibited by old untreated rats towards those of the young ones (Supplementary Fig. 13 and Supplementary Table S7). This is easily visualized by the movement of the orange dots, representing treated old rats in each graph towards the blue dots, representing young rats. Plasma fraction treatment has not caused any changes to the blood indices that would indicate any organ dysfunction. Instead, it rejuvenated the blood of the rats, which is consistent with the significant reduction of epigenetic age of their blood as measured by both the rat multi-tissue and blood clocks.

Biomarkers for vital organs

To ascertain the impact of plasma fraction treatment on vital organs, we measured the levels of the following biomarkers on 30, 60, 90, 120, and 155 days from the start of the experiment: bilirubin, serum glutamic-pyruvic transaminase (SGPT), and serum glutamic-oxaloacetic transaminase (SGOT) to monitor liver function; triglycerides (TG), high-density lipoprotein (HDL) and total cholesterol to monitor risk of atherosclerosis and heart disease, and liver function as well; glucose to monitor the pancreas and diabetes; and creatinine and blood urea nitrogen for kidney function. The levels of all these biomarkers in the treated old rats were altered towards the values of young rats, without exception (Fig. 3 and Supplementary Table S8). This is easily visualized by the movement of the orange dots, representing treated old rats in each graph towards the blue dots, which represent young rats. Collectively, these results show that the functions of all the vital organs tested through their respective biomarkers were rejuvenated by E5 treatment. This is entirely consistent with reversal of the epigenetic ages of their hearts and livers.

Fig. 3

Assessment of plasma fraction treatment on vital organ functions. At 0, 30, 60, 90, 120, and 155 days from commencement of the experiment, the health and function of vital organs (liver, heart, kidney, and pancreas) of six rats per group were monitored through measurements of appropriate biomarkers. SPGT, serum glutamic-pyruvic transaminase; SGOT, serum glutamic-oxaloacetic transaminase; HDL, high-density lipoprotein; and BUN, blood urea nitrogen. Red dots represent data points of old rats, orange dots represent treated old rats, and blue represent young rats. Each data point represents average values from six rats with two standard errors around the mean. Detailed measurements of each parameter are provided in Supplementary Table S8
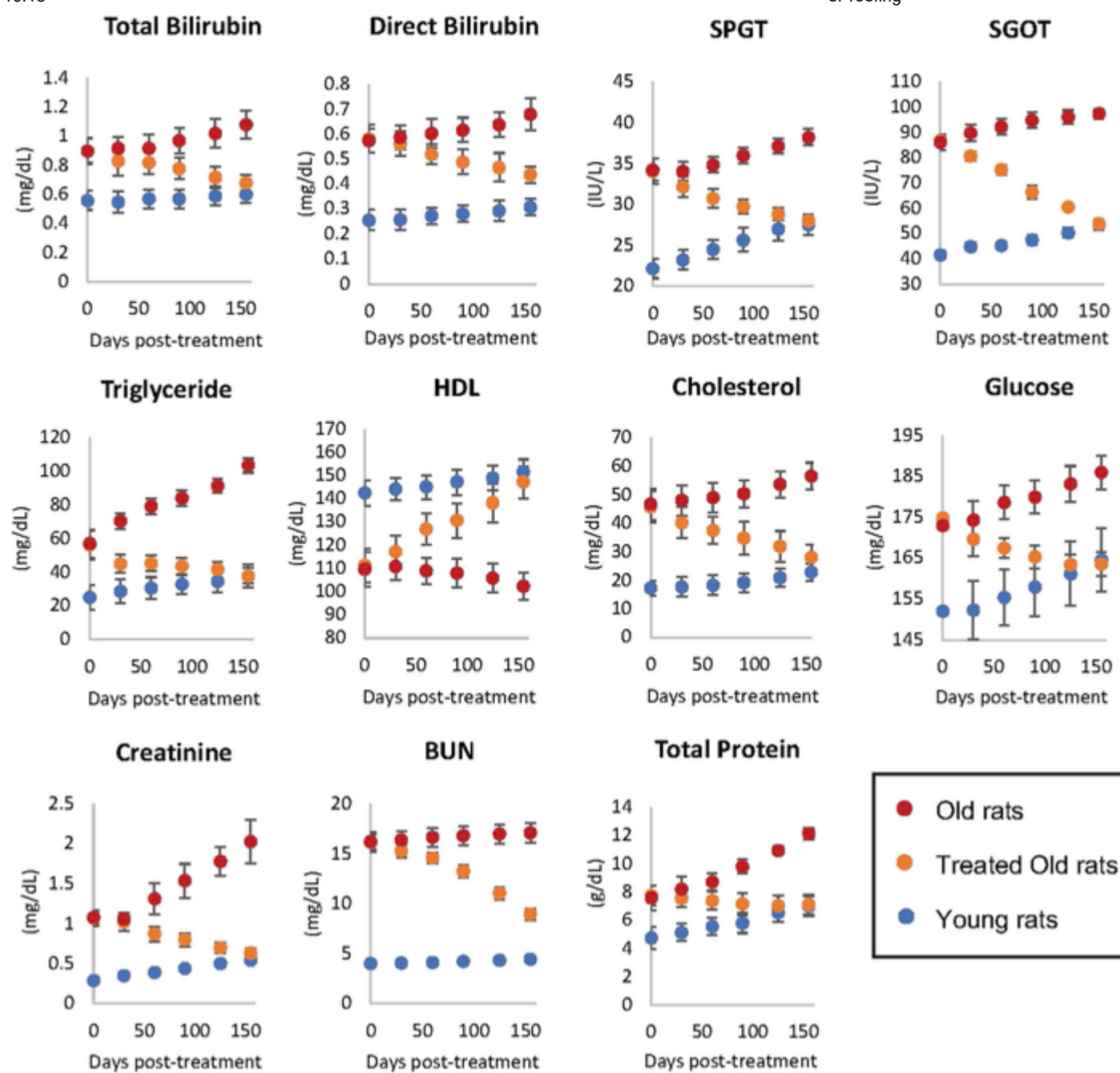
We advise readers to be aware that biomarker measurements in rat vital organs can differ significantly in values and patterns compared to humans. What may be detrimental in one species could be inconsequential in another. This discrepancy is a significant limitation observed not just in vital organ biomarkers but also in many other aging-related clinical biomarkers. Such differences can elucidate why numerous rejuvenation treatments do not effectively transition from rodents to humans. In contrast, epigenetic clocks, particularly those designed for multiple species, maintain relevance across different species simultaneously.

Cognitive function

Learning and memory, which are constituent characteristics of cognitive functions, decline not only in humans but also in rats, starting from 12 months of age [38]. Barnes maze was used to measure the latency period required by the rats to escape through the right hole into an escape box. Videos illustrating the latency pattern of three rats (young, old treated, old untreated) can be found in the Supplement.

In this study, the animals received the E5 dosage regimen two times: the first at the beginning of the trial and the second on the 96th day of the study. Compared to the first month, there was a greater difference in cognitive performance between the treated animals and the untreated control group during the third and fourth months (Fig. 4). This suggests that the cumulative effect of the two doses played a crucial role in enhancing cognitive function.

Fig. 4

Assessment of plasma fraction treatment on cognitive function (learning and memory). Rats were subjected to Barnes maze test in the first to fourth month from commencement of the experiment. Each assessment consists of nine consecutive days of test where the time (in seconds) required by the rats to find the escape hole (latency) was recorded and plotted. In this study, the animals received the E5 dosage regimen two times: the first at the beginning of the trial and the second on the 96th day of the study. We noticed a distinct change in specific months where the cognitive performance of the treated animals appears to start out similar with that of the non-treated group (during the first 2 months, red and orange lines in the upper right panel). This is despite differences observed between these two groups in the previous month (separated red and orange curves in the upper left panel). This complex pattern reflects that latency evidently rebounded within the 3-week span. A comparable observation can be made for the lower two panels (3rd and 4th months). The error bars depict two standard errors
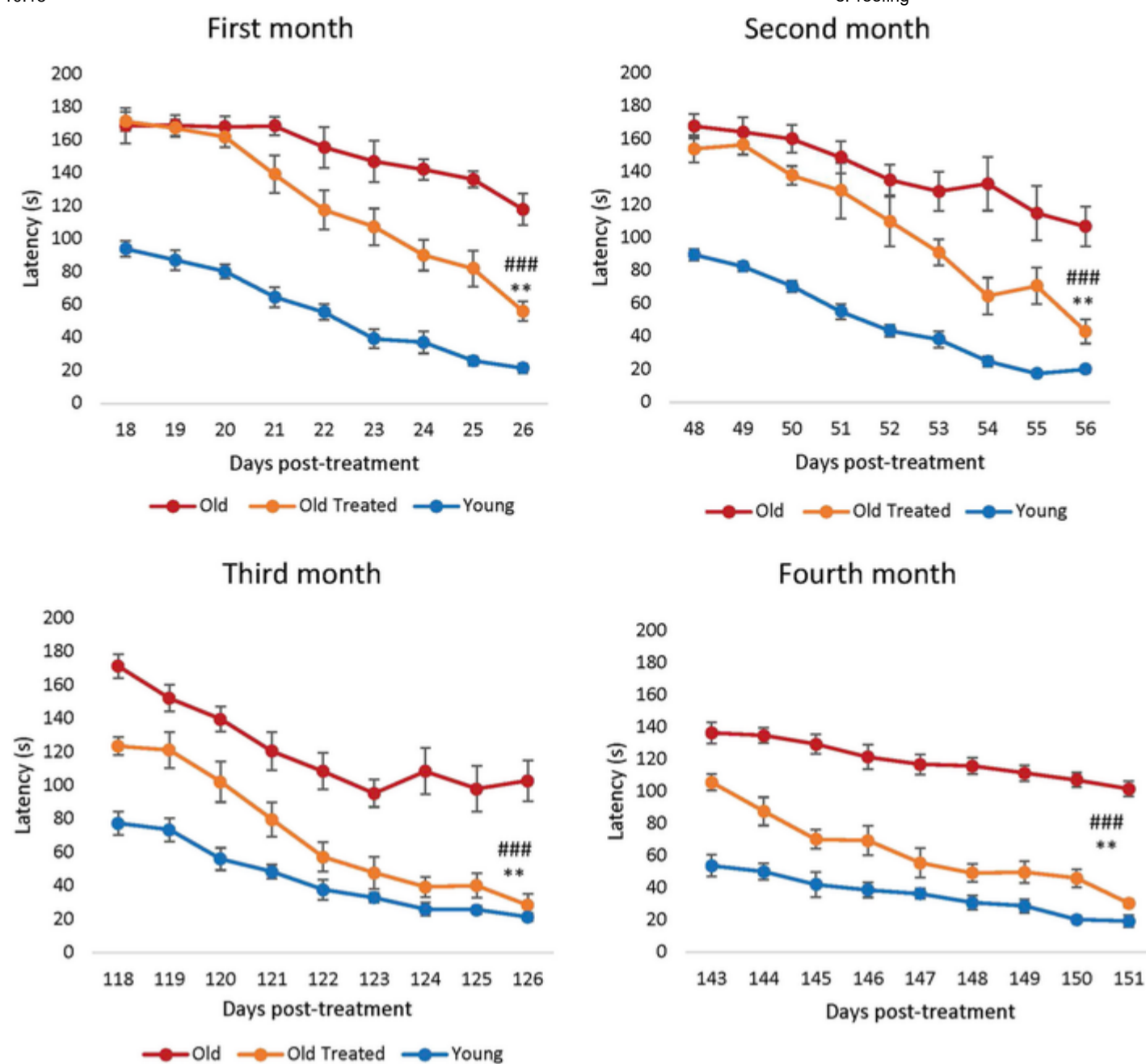
Within a month of plasma fraction treatment, the rats exhibited significantly reduced latency to escape (Fig. 4), i.e., they learned and remembered better.

After the second month, the treated rats began with a slightly reduced latency period compared to the untreated old rats, and once again, they learned much faster than the latter. By the third month, it was clear that treated rats remembered the maze much better than the untreated ones even from the first day of test as their latency period was significantly reduced and by the end of the test period, their latency was like that of the young rats. This feature was sustained and repeated in the fourth month.

Collectively, these results show that E5 improved the learning and memory of the rats. Interestingly, the epigenetic age of treated rat brain samples (hypothalamus) was lower than the untreated old ones, but less markedly than the magnitude of decrease of epigenetic age of the blood, heart, and liver. This introduces numerous possible insights into the relationship between cognitive function, biological age, and physical health which will be further elaborated in the " Discussion ."

Cellular stress

There is no doubt that the reduction in epigenetic age of liver, heart, brain, and blood by plasma fraction was accompanied by startling improvement in the function of these organs. In addition to the decline of organ function with age is the rise of two cell stress features which are related, namely oxidative stress and chronic inflammation; the excess of which have been linked to multiple pathologies. We carried out a panel of biomarker tests for these two features in the test rats.

Oxidative stress

Oxidative stress results from the excess of reactive oxygen species (ROS) in cells. This situation can arise due to the over-production of ROS or the decline in the ability to remove or neutralize ROS. While ROS at low levels are not harmful and can even be necessary, at higher concentrations, they can interact with biomolecules like lipids and impair their function. Measuring the levels of malondialdehyde (MDA), which is the end-product of polyunsaturated fatty acid peroxidation, reveals the levels of cellular ROS. The amounts of MDA were clearly higher in the brain, heart, lung, and liver of older rats (Fig. 5), and plasma fraction treatment reduced this level to that of young rats. Hence, regardless of the source of augmented ROS in older rats, plasma fraction appears to be able to reduce it effectively.

Fig. 5

Assessment of plasma fraction treatment on oxidative stress. At the end of the experimental period of 155 days, lipid peroxidation level, which is an indicator of intracellular level of reactive oxygen species (ROS), was determined by measuring the amount of malondialdehyde (MDA), which is the end-product of polyunsaturated fatty acid peroxidation. The levels of three antioxidants: reduced glutathione, catalase, and superoxide dismutase levels were also measured to ascertain the impact of plasma fraction treatment on oxidative stress. Detailed values are reported in Supplementary Table S9 . The error bars depict two standard errors

Malondialdehyde (MDA)

Reduced Glutathione (GSH)

Catalase

Superoxide Dismutase
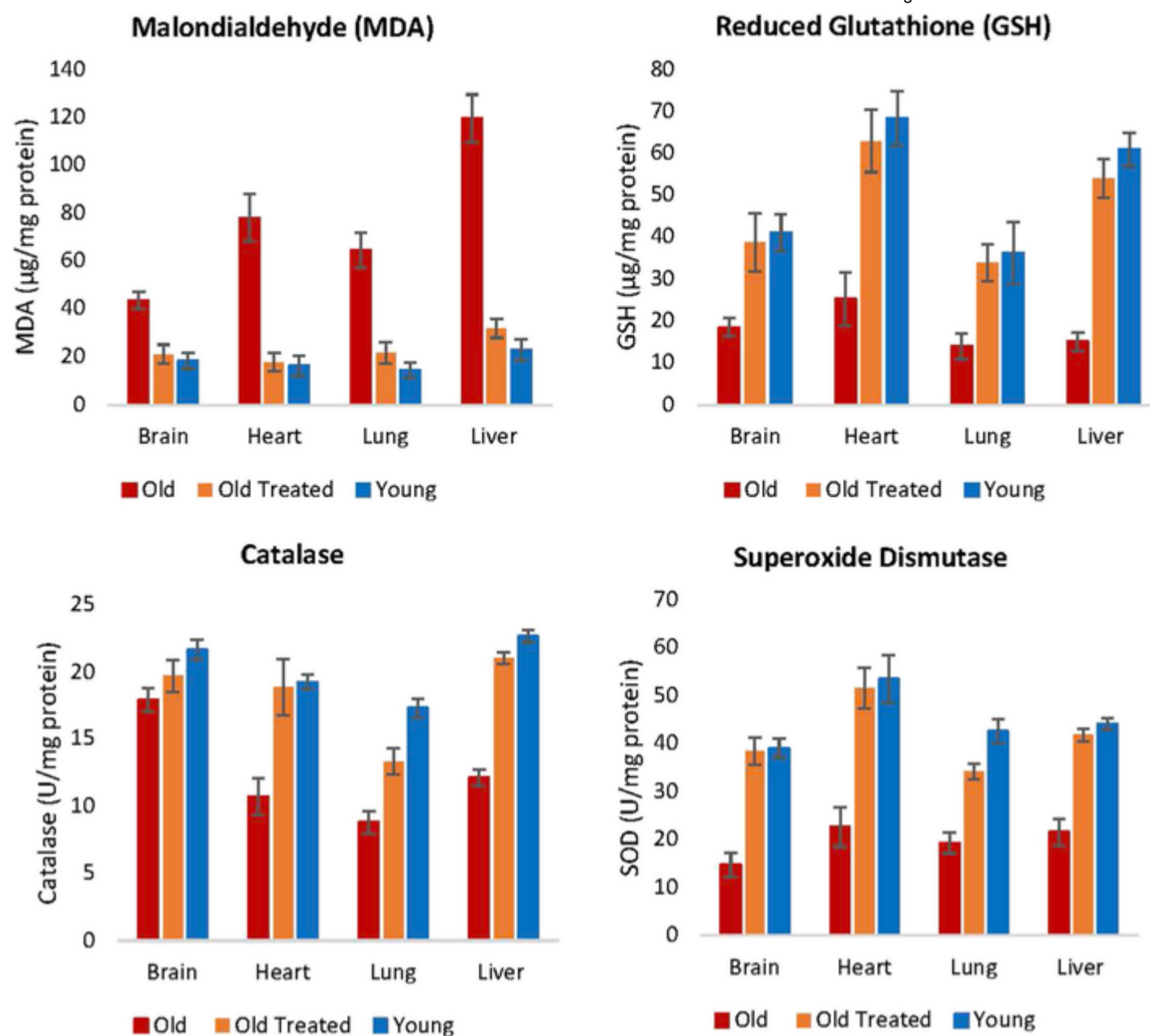
Apart from increased production of ROS, decreased efficiency in eliminating ROS also contributes to the age-associated rise in its level. ROS are neutralized by cellular antioxidants including but not limited to reduced glutathione, catalase, and superoxide dismutase, which all work in very different ways. The levels of these three antioxidants were reduced in tissues of old untreated rats but the plasma fraction treatment augmented them to levels that are comparable to young ones (Fig. 5).

Our findings revealed that E5 significantly elevated the levels of glutathione (GSH) and the concentration of superoxide dismutase (SOD) in all four examined rat tissues: brain, heart, lung, and liver (Student's T $p < 0.05$, Supplementary Table S9). In contrast, malonaldehyde levels, indicative of lipid oxidation by ROS, were significantly ($p < 0.05$) reduced to those observed in young controls across all these organs when examined ex vivo. Furthermore, E5 led to a significant rise in catalase levels in the heart, lung, and liver, though no such increase was observed in the brain. Collectively, these findings underscore E5's potential in restoring oxidative stress markers in aged rats to levels comparable to their younger counterparts.

It remains to be ascertained if the reduction of ROS levels, as measured by MDA, was due entirely to the increase in the amounts of antioxidants, or whether plasma fraction treatment also induced a concomitant reduction in the production of ROS from multiple and various intracellular sources. Nevertheless, the endpoint of ROS levels in old rats being diminished to the level of young ones is yet another indication of the rejuvenating effect of the treatment.

Chronic inflammation

Inflammation is an important response that helps protect the body, but excess inflammation especially in terms of duration of this response can have very detrimental effects instead. This occurs when inflammation fails to subside and persists indefinitely, a condition referred to as chronic inflammation, which, for reasons not well-understood, increases with age and is associated with a multitude of conditions and pathologies. The levels of two of the most reliable and common biomarkers of chronic inflammation: interleukin-6 (IL-6) and tumor necrosis factor-α (TNF-α) are found to be considerably higher in old rats (Fig. 6), and these were very rapidly diminished, within days by E5 treatment, to comparable levels with those of young rats. This was especially stark with IL-6. The reduction of these inflammation markers is consistent with the profile of the nuclear factor erythroid 2-like 2 protein (Nrf2), which plays a major role in resolving inflammation, in part by inhibiting the expression of IL-6 and TNF-α. Nrf2 also induces the expression of antioxidants that neutralizes ROS, which is also a significant feature in inflammation [41]. In summary, plasma fraction reduces oxidative stress and chronic inflammation, which are age-associated pan-tissue stresses, to the levels found in young rats.

Fig. 6

Assessment of the effect of plasma fraction treatment on chronic and systemic inflammation. Blood levels of interleukin-6 (IL-6) and tumor necrosis factor-α (TNF-α) were measured at regular intervals throughout the 155-day period of the experiment. At the end of the experiment, the levels of Nrf2, a pivotal modulator of inflammation, and oxidative stress were measured in brain, heart, lung, and liver of the rats. Detailed values of IL-6, TNF-alpha, and Nrf2 can be found in Supplementary Table S10, Supplementary Table S11, and Supplementary Table S12. The error bars depict two standard errors
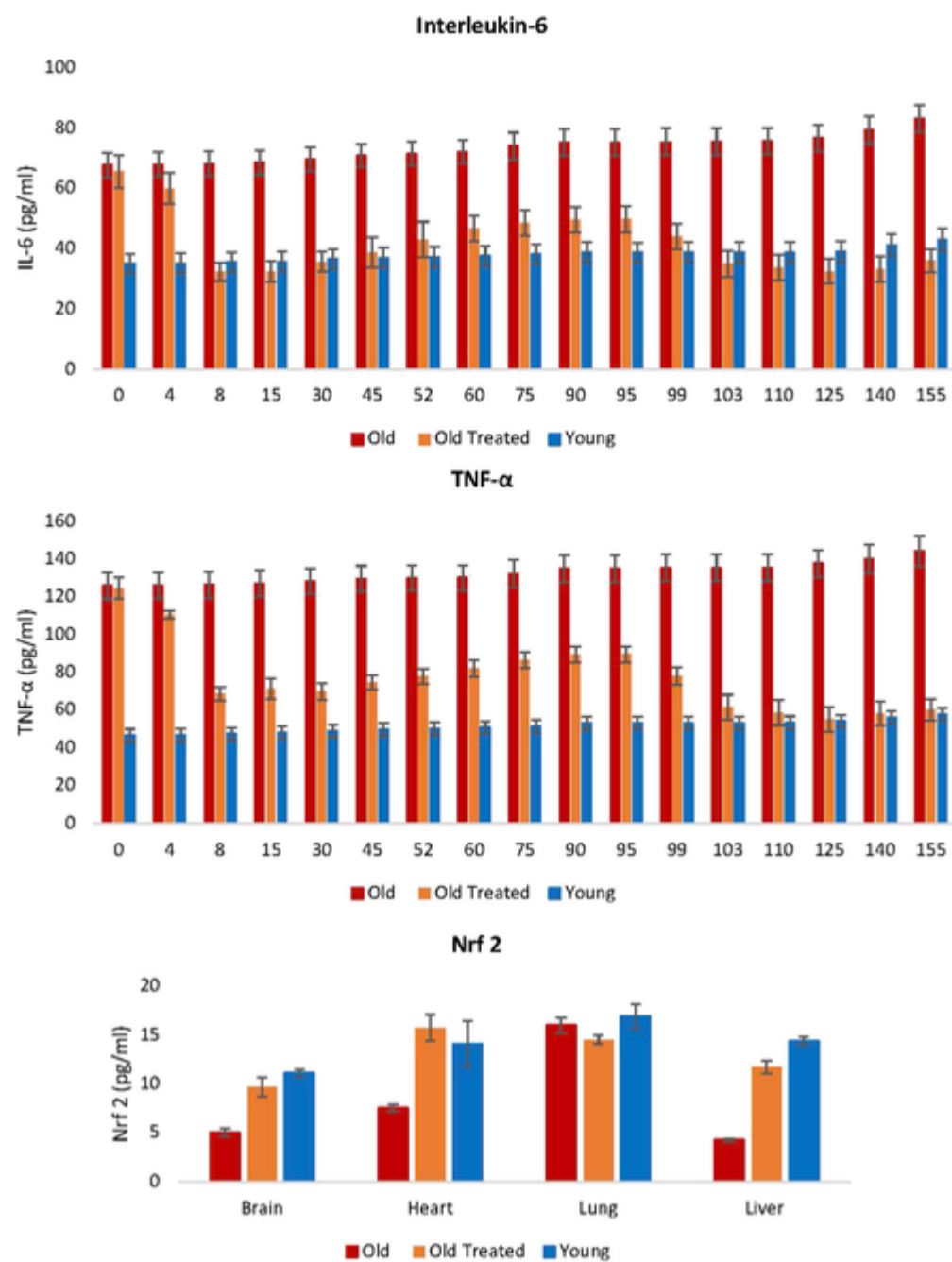
Rationale for administering a second E5 dose

Fig. 6 illustrates the temporal progression of inflammatory cytokines IL-6 and TNF-alpha levels. In time, the levels of the two inflammatory factors began to rise gradually, but they were once again very effectively reduced following the second administration of E5 on the 95th day. After initially declining to levels comparable to our young controls 2 weeks post the initial E5 injection, these levels plateaued for several weeks. However, they subsequently surged at a pace surpassing that of our young controls. Following a secondary treatment regimen, which entailed a series of E5 intravenous injections initiated 95 days post the initial treatment, the cytokine levels dipped below those of our young controls. It is noteworthy that during this treatment period, our young controls aged (considering 2.5 weeks of rat life roughly equates to a human year, though the correlation is not strictly linear). Post this treatment, the rise in inflammatory cytokines mirrored that of the young controls.

We hypothesize that the initial rejuvenation witnessed an accelerated aging effect, in terms of inflammatory cytokine levels, due to the presence of pro-aging factors in the older test subjects. However, during the second rejuvenation phase, these factors were absent, allowing the aging process, and consequently the cytokine levels, to align with that of our young controls. Our results suggest the existence of tissue- and cell-specific aging states which can be recalibrated by E5 components to reflect a "young adult" state. Once adjusted, aging resumes at a species-typical rate. The ability to recalibrate aging states, as demonstrated by our second rejuvenation treatment, is a noteworthy insight.

Additional validation: E5 works in both sexes

The pronounced rejuvenation effects in male rats prompted us to conduct further confirmatory experiments. A particularly important consideration is the effectiveness of E5 with regard to sex, as sex-dependent rejuvenations by some interventions have previously been reported [42]. To assess E5's applicability to both male and female Sprague-Dawley rats, we studied 12 males (six treated with E5, six with saline) and 12 females (six treated with E5, six with saline). These rats were treated every 45 days with an injection of E5 or saline. The rats were monitored for 165 days, and blood was drawn at six time points: 0, 15, 30, 60, 150, and 165 days from the first injection (Supplementary Fig. 14). We observed substantial improvements in IL-6 and TNF-alpha levels in the blood of both sexes within 15 days of the first injection of E5 (Student's T test $p < 0.05$, Supplementary Fig. 14). At the end of the study (165 days), after three dosing cycles of E5, we observed highly significant improvements in TNF-alpha levels (Student's T test $p = 1.3 \times 10^{-6}$ for males and $p = 7.6 \times 10^{-5}$ for females) and IL-6 levels ($p = 4.1 \times 10^{-6}$ for males, $p = 3.4 \times 10^{-6}$ for females, Supplementary Fig. 14 A–D) in the blood of E5-injected rats over that of saline controls. We also observed a substantial improvement in grip strength ($p = 6.8 \times 10^{-7}$ for males, $p = 4.6 \times 10^{-6}$ for females, Supplementary Fig. 14 E,F). Our study shows age reversal effects in both male and female rats, but E5 is more effective in males.

Second E5 methylation experiments in blood

To validate our epigenetic clock results, we conducted a second set of E5 experiments with Sprague-Dawley rats of both sexes. When these rats turned 26 months old, half (nine rats) received the E5 treatment while the other half (eight rats) received only the control

treatment (saline injection). We analyzed methylation data from two blood draws: blood draw before treatment (baseline) and a follow-up sample (15 days after the E5/saline treatment).

Again, we observed significant rejuvenation according to the final rat clock for blood (two-sided Kruskal-Wallis $p = 0.0094$, Supplementary Fig. 15 A,B), and the final pan-tissue clock ($p = 0.054$, Supplementary Fig. 15 C,D). After omitting an outlying control sample, we obtained more significant results in both sexes ($p = 0.00086$, $p = 0.014$ in females, $p = 0.053$ in males, Supplementary Fig. 15 F–J).

Our results are consistent with the results from a different evaluation of young whole plasma extracted from young rats. In this study, whole plasma from young rats (2 months) was intraperitoneally injected into 25-month-old rats until their natural death [43]. As in the current study, this separate investigation using whole plasma also found that very soon following treatment, the DNAm age of the treated rats fell below that of controls and remained lower until the end of their lives [43].

Evaluation immunoglobulin G N-glycan aging

The pivotal function of IgG N-glycosylation in the realms of immunity and inflammation correlates its modifications with inflammaging — a foundational theme in age-related diseases [44]. Until now, the glycan aging clock, informed by the glycomics of IgG, has been employed as an indicator of biological aging exclusively in humans.

In this study, we expanded upon this framework and leveraged glycoproteomics to determine the impact of E5 treatment on the glycan aging of rat IgG. We recorded alterations in rat IgG Fc N-glycosylation for subclasses IgG2a, IgG2b, and IgG2c at two distinct timepoints. Among the control group of untreated rats, we noticed an escalation in IgG agalactosylation (IgG2a-G0) and a reduction in digalactosylation (IgG2a-G2). This overarching pattern mirrors the typical trend observed during human biological aging (Fig. 7 and Supplementary Table S13).

Fig. 7

Plasma fraction treatment induces a shift from pro- to anti-inflammatory glycan aging pattern in rat IgG2a N-glycoproteomics. Following the administration of the third E5 dose, rat serum was sampled on the fifteenth day for subclass-specific immunoglobulin G (IgG) Fc N-glycosylation analysis using nano-LC-MS. Notably, a significant ($p < 0.05$) reduction in the relative abundance of the pro-inflammatory agalactosylated IgG2a glycoform (G0) was recorded. This was accompanied by a simultaneous upsurge in the anti-inflammatory digalactosylated glycoform (G2). The glycoproteomic data was evaluated using a linear mixed-effects model. Median values are emphasized in black (for controls) or red (for treatment) at each time point, with the relative change being normalized to baseline. N-glycan illustrations are provided, utilizing the symbol nomenclature endorsed by the Consortium for Functional Glycomics. Detailed values can be found in Supplementary Table S13
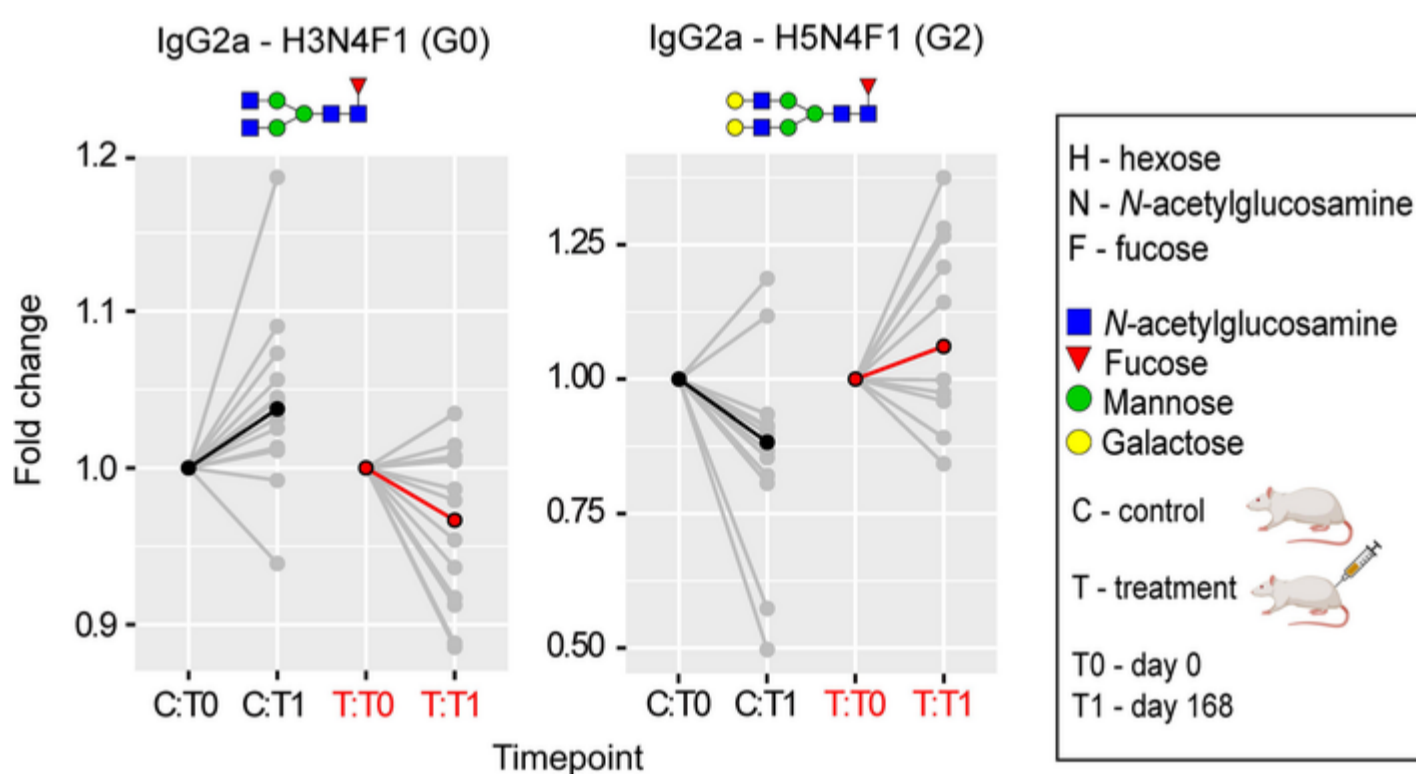
On the fifteenth day after administering the third dose of E5, rat serum was collected for subclass-specific IgG Fc N-glycosylation analysis using nano-LC-MS. We observed a significant ($p < 0.05$) decrease in the relative abundance of the pro-inflammatory agalactosylated IgG2a glycoform (G0), which was accompanied by a corresponding surge in the anti-inflammatory digalactosylated glycoform (Fig. 7 and Supplementary Table S13). While IgG monogalactosylation (IgG2a-G1) also adheres to this trend in the E5-treated group of rats (Supplementary Table S13), this glycoform exhibits a stronger correlation with specific diseases and general health rather than aging [37].

Contents of E5

Blood is known to contain a diverse range of exosome types. Since the contents of exosomes mirror their cells of origin, they can encapsulate a variety of proteins, growth factors, and RNA species, including mRNA, miRNA, piwiRNA, siRNA, lncRNA, and circRNA, among others [45].

For our exosome precipitation process, we utilized the modified Extra-PEG method. Adapted from virus separation techniques, this method has shown to be more effective in exosome precipitation than traditional methods. Specifically, using PEG 6000 at an 8%

concentration yielded a higher exosome concentration. To further enhance exosome enrichment, we increased this concentration to 12%, although this led to a higher protein-to-exosome ratio [46]. To ensure the capture of extracellular vesicles (EVs) of all sizes, such as small exosomes, exomeres, and supermeres, we opted for the higher PEG concentration. This approach is designed to precipitate both smaller particles, like small exosomes, and larger ones, including large exosomes and ectosomes.

Exosomes are a specific subtype of extracellular vesicles. They can be distinguished by several characteristics, such as their particle size —typically ranging from 30 to 150 nm in diameter—and the presence of specific proteins. Notably, exosomes often contain tetraspanins, including CD63 and CD81 [47].

In our study, we analyzed the E5 sample based on these characteristics. Our primary objective was to identify both low and high molecular weight RNA. We extracted RNA from a 400 µl E5 sample and then conducted gel electrophoresis, as detailed in the Supplementary Methods. The electrophoresis results (Supplementary Fig. 16) showed two distinct bands: one at 100 base pairs and another significantly above 1000 base pairs. RNAs with lengths exceeding 1000 base pairs are typically classified as long-chain non-coding RNAs (lncRNAs). This suggests that the E5 samples are predominantly composed of lncRNAs.

Furthermore, we utilized Western blots to confirm the presence of CD63 and CD81 proteins in the E5 sample (Supplementary Fig. 17).

Future research should delve deeper into exosomal contents. Existing studies have already identified an extensive range of proteins, miRNAs, mRNAs, lipids, and metabolites within exosomal cargo [45, 46].

Discussion

Decades ago, parabiosis experiments revealed the potential of young circulation in benefiting older mice and rats' organ function. More recent work has begun to leverage this fascinating discovery for medical applications [5, 6, 7, 8, 9, 10, 11, 12, 39, 40]. The early presumption was that this improvement not only signifies rejuvenation, but it also could represent functional enhancements without altering epigenetic state or age. This ambiguity underlined the question: what is aging?

Our study presents compelling evidence for epigenetic age reversal in rats via the administration of exosome-containing fraction derived from plasma of young adult pigs. Following our initial report in 2020 [48], additional validation and cross-species evidence affirmed our results [43, 49, 50, 51]. Mice studies confirmed that young plasma, administered through heterochronic parabiosis, rejuvenated solid organs, reduced epigenetic age by up to 30%, and extended both lifespan and healthspan, with the effect persisting post-separation [50].

Given the limitations of mouse models for extensive blood collection, we developed six rat-specific epigenetic clocks using DNA methylation data from thirteen tissue types, aligning with our Mammalian Methylation Consortium's pan-mammalian clocks [52]. This research encompassed creating rat-specific clocks, studying plasma fraction treatment effects on epigenetic age, and investigating its impact on aging biomarkers, including a novel rat-specific biomarker for immunoglobulin G N-glycan aging.

Despite disparate data distribution between species with different lifespans, we managed to establish a human-rat pan-tissue relative age clock, offering biologically significant values by displaying relative biological age within each species. Utilizing a mammalian DNA methylation array profiling 36,000 conserved probes across various mammalian species was crucial in achieving this.

E5 treatment exhibited great potential, significantly reducing epigenetic ages across multiple rat organs, reduced markers of chronic inflammation and oxidative stress, and increased antioxidant levels. These features are particularly important because oxidative stress and inflammation are two fundamental physiological processes underlying many different types of pathologies [53, 54]. Interestingly, the effect of E5 on the brain is modest. This is possibly due to slower tissue turnover [55, 56], but a more certain answer can only be found when a better understanding of the mechanism of epigenetic aging is known. Our current understanding of this mechanism points to a close relationship with development and homeostatic body maintenance post-maturity [27, 56, 57, 58, 59, 60, 61, 62]. Regardless of the reason, maze test performance demonstrated improved brain function of E5-treated rats. Whether this reflects healthier brain function due to overall physical improvements or actual molecular brain rejuvenation remains to be explored.

The mechanism of reversing glycan aging is not entirely clear yet, but our previous studies suggested a potential involvement of IL-6 and TNF-α [53, 54]. The observed reduction in these concentrations, coupled with the reversal of pro-inflammatory IgG glycosylation pattern following treatment, supports the rejuvenating impact of E5.

We found the plasma fraction treatment consistently effective in both male and female rats, drastically reducing the epigenetic age of multiple rat tissues. This suggests a potential paradigm shift in healthcare; rather than treating diseases individually, rejuvenation may systemically reduce disease onset risk.

Our study showcased E5 treatment's rejuvenating capacity in old rats with just two series of injections. The systemic rejuvenation of non-blood organs and the reversal of the epigenetic clock suggests a promising strategy for disease prevention. While E5 treatment is yet to undergo human trials, there is room for optimism as umbilical cord plasma concentrate-based treatment has demonstrated promising effects in a phase 1 clinical trial [51]. In this regard, our use and demonstration of the rejuvenating efficacy of plasma fraction from young adult pigs is noteworthy. Not only does this reinforce the universality of the aging process in different mammalian species, but it also demonstrates that the source of the rejuvenating material can be readily obtained from species other than humans, which will greatly address the issue of supply, economics, and ethics, which would otherwise be highly challenging.

We would like to conclude our discussion by theorizing about the possible mechanisms that connect our findings. By adjusting the epigenome, the aging process can be accelerated or reversed [63].

Our study indicates that transferring plasma between species, specifically between pigs and rats, can rejuvenate certain tissues. Such findings offer insights into shared biological mechanisms across species, which are potentially relevant to human health. The mechanism behind E5's effects is intriguing. The cellular secretome, which E5 taps into, changes as mammals get older. While a comprehensive list of

these changes is beyond this paper's scope, one notable change is the reduction in longer transcripts with age [64]. This same paper points out that these longer transcripts are associated with genes known to prolong lifespan. Our research found that E5 contains lncRNAs. Thus, introducing E5 to older mammals could address the transcript size disparity seen with aging. It is noteworthy that many of these regulatory molecules in the secretome are conserved across mammals.

We posit that E5 rejuvenation's primary drivers are nanoparticles and their contained cargo. A vast array of proteins, miRNAs, mRNAs, and lipids have been identified in exosomal cargo. Known as EVs, exosomes are ubiquitous in cells, tissues, and bodily fluids. They engage with target cells, get internalized, and can even extend lifespan. Exosomes can stimulate antitumor activity, promote tissue regeneration, and even cross the blood-brain barrier. Their role in cell communication, development, immune response, and tissue repair is vital, especially as these functions decline with age.

Materials and methods

Materials

In total, we analyzed $n = 613$ rat tissue samples from 13 different tissues/organs (Supplementary Table S1 , Supplementary Table S2 , Supplementary Table S3). Ages ranged from 0.0384 years (i.e., 2 weeks) to 2.3 years (i.e., 120 weeks). The rat data were comprised of a training set ($n = 503$, Fig. 1 , Supplementary Table S1), a test set for the E5 treatment ($n = 76$ from multiple tissues, Fig. 2 , Supplementary Table S3) and a second test set for the E5 treatment ($n = 34$ from blood, Supplementary Table S3).

We used $n = 503$ tissue to train four clocks: a pan-tissue clock based on all available tissues, a brain clock based on regions of the whole brain — hippocampus, hypothalamus, neocortex, substantia nigra, cerebellum, and the pituitary gland, a liver clock based on all liver samples, and a blood clock.

To build human-rat clocks, we added $n = 1366$ human tissue samples to the training data. We first trained/developed epigenetic clocks using the training data ($n = 503$ tissues, Supplementary Table S1). Next, we evaluated the data in independent test data ($n = 76$ for evaluating the effect of E5 plasma fraction treatment (Supplementary Table S3).

Methods

The rat tissues came from four different labs across three countries: (i) India: Yuvan Research in collaboration with School of Pharmacy SVKM's NMIMS University (K. Singh), (ii) USA: University of Tennessee Health Science Center (H. Chen) and Medical College of Wisconsin (L. C. Solberg Woods), and (iii) Argentina: University of La Plata (R. Goya).

Rats from Tennessee and Wisconsin

Blood samples ($n = 48$): Male and female heterogeneous stock rats were bred at the Medical College of Wisconsin (Solberg Woods Lab) or University of Tennessee Health Science Center (Hao Chen Lab). Heterogeneous stock (HS) populations were originally developed by breeding together eight inbred strains, followed by maintaining the colony in a manner that minimizes inbreeding, allowing fine-resolution genetic mapping of a variety of complex traits [65]. Rats were euthanized at different ages by an overdose of isoflurane (> 5%). Trunk blood was collected immediately and stored at −80 °C until processing. Blood samples were treated with streptokinase (60–80 IU/200 μl blood, overnight incubation at 37 °C) and DNA was extracted using the QiaAmp Blood Mini Kit (Qiagen Cat No./ID: 51304) following manufacturer's instructions. All procedures were approved by the Institutional Animal Care and Use Committee of the University of Tennessee Health Science Center or the Medical College of Wisconsin and followed the NIH Guide for the Care and Use of Laboratory Animals. Genomic DNA was isolated from tissue samples mostly using Puregene chemistry (Qiagen). DNA from liver was extracted manually and from blood using an automated Autopure LS system (Qiagen). From tissues and clotted blood samples, DNA was extracted manually using QiaAmp DNA Blood Midi Kit and the DNeasy Tissue Kit according to manufacturer's protocol (Qiagen, Valencia, CA). DNA from BA10 was extracted on an automated nucleic acid extraction platform Anaprep (Biochain) using a magnetic bead-based extraction method and Tissue DNA Extraction Kit (AnaPrep).

Rats from the University of La Plata (R. Goya lab)

Multiple tissues/cell types were studied, including adipose, blood, cerebellum, hippocampus, hypothalamus, liver, neocortex, ovaries, pituitary, skin, and substantia nigra. We used female Sprague-Dawley (SD) rats, raised in our institute, across various age groups: young (3.7 months, $n = 11$), late adults (LA, 8.0 months, $n = 9$), middle-aged (M-A, 15.7 months, $n = 6$), and old (25.5 months, $n = 14$). Animals were housed in a temperature-controlled room (22 ± 2 °C) on a 12:12 h light/dark cycle. Food and water were available ad libitum. All experiments with animals were performed in accordance with the Animal Welfare Guidelines of NIH (INIBIOLP's Animal Welfare Assurance No. A5647-01) and approved by our Institutional IACUC (Protocol # P05-02-2017).

Tissue sample collection Before sacrifice by decapitation, rats were weighed, blood was withdrawn from the tail veins with the animals under isoflurane anesthesia and collected in tubes containing 10 μl EDTA 0.342 mol/l for 500 μl blood. The brain was removed carefully severing the optic and trigeminal nerves and the pituitary stalk (not to tear the pituitary gland), weighed, and placed on a cold plate. All brain regions were dissected by a single experimenter (see below). The skull was handed over to a second experimenter in charge of dissecting and weighing the adenohypophysis. The rest of the body was handed to other two or three experimenters who dissected and collected whole ovaries, a sample of liver tissue, adipose tissue, and skin tissue from the distal portion of tails.

Brain region dissection Prefrontal cortex, hippocampus, hypothalamus, substantia nigra, and cerebellum were rapidly dissected on a cold platform to avoid tissue degradation. After dissection, each tissue sample was immediately placed in a 1.5 ml tube and momentarily immersed in liquid nitrogen. The brain dissection protocol was as follows. First a frontal coronal cut was made to discard the olfactory

bulb, then the cerebellum was detached from the brain and from the medulla oblongata using forceps. To isolate the medial basal hypothalamus (MBH), brains were placed ventral side up and a second coronal cut was made at the center of the median eminence (−3.6 mm referred to bregma). Part of the MBH was taken from the anterior block of the brain and the other part from the posterior block in both cases employing forceps. The hippocampus was dissected from cortex in both hemispheres using forceps. This procedure was also performed on the anterior and posterior blocks, alternatively placing the brain caudal side up and rostral side up. To dissect the substantia nigra, in each hemisphere, a 1-mm thick section of tissue was removed from the posterior part of the brain (−4.6 mm referred to bregma) using forceps. Finally, the anterior block was placed dorsal side up, to separate prefrontal cortex. With a sharp scalpel, a cut was made 2 mm from the longitudinal fissure, and another cut was made 5 mm from it. Additionally, two perpendicular cuts were made, 3 mm and 6 mm, from the most rostral point, obtaining a 9 mm^2 block of prefrontal cortex. This procedure was performed in both hemispheres and the two prefrontal regions collected in a code-labeled tube.

Anterior pituitary   Using forceps, the dura matter that covers gland was removed leaving the organ free on the sella turcica. The neural lobe was carefully separated from the anterior pituitary (AP) which was then carefully lifted with fine curved tip forceps pointing upwards. It was rapidly weighed, then put in a tube and placed momentarily in liquid nitrogen.

Ovaries   The genital apparatus was dissected by cutting the mesentery to isolate the uterine horns, the tubular oviduct, the ovaries, and the junction between the anus/rectum and the vulva/vagina, leaving the unit of the sexual organs and the urinary bladder isolated. The ovaries were carefully separated from the oviducts; the fat around the ovaries was also removed. Both gonads were placed in a single Eppendorf tube and momentarily placed in liquid nitrogen.

Liver   Liver tissue extraction was made by cutting a piece of the median lobe (0.5 cm × 0.5 cm). Tissue was placed in a tube and momentarily stored immersed in liquid nitrogen.

Adipose tissue   Adipose tissue samples were obtained from the fatty tissue of the small intestine.

Tail skin   For skin tissue, 5 cm of a distal tail portion were cut with scissors. Skin was separated and hair removed using scalpel. Tissue was placed in a tube and stored as described for other tissues.

DNA was extracted from blood on an automated nucleic acid extraction platform called QiaSymphony (Qiagen) with a magnetic bead-based extraction kit, QIAsymphony DNA Midi Kit (Qiagen). DNA was extracted from tissue on an automated nucleic acid extraction platform called Anaprep (Biochain) with a magnetic bead-based extraction kit, Tissue DNA Extraction Kit (Biochain). DNA from brain regions was extracted using an automated nucleic acid extraction platform called QIAcube HT (Qiagen) with a column-based extraction kit, QIAamp 96 DNA QIAcube HT Kit (Qiagen).

Rats from Yuvan Research Group

The Sprague-Dawley rats were procured from the National Institute of Bioscience, Pune, India. Animals were housed in the animal house facility of School of Pharmacy, SVKM's NMIMS University, Mumbai during the study under standard conditions (12:12 h light: dark cycles, 55–70% of relative humidity) at 22 ± 2 °C temperature with free access to water and standard pellet feed (Nutrimix Std-1020, Nutrivet Life Sciences, India). The animals were acclimatized to laboratory environment for 7 days before initiation of the study. The experimental protocol was approved by the Institutional Animal Ethics Committee. The approval number is CPCSEA/IAEC/P-75/2018.

Sprague-Dawley rats of both sexes were used, from which blood, whole brain, heart, and liver were harvested. Three batches or samples were prepared.

The first batch was intended for training the epigenetic clock: $n = 42$ blood samples, $n = 18$ whole brain, $n = 18$ heart, $n = 18$ liver samples.

The second batch of test set involved $n = 76$ tissue samples from male rats ($n = 22$ blood, $n = 18$ liver, $n = 18$ heart, $n = 18$ hypothalamus). The test data were used to evaluate the effect of the treatment in three conditions: young (30 weeks old) and treated old samples (109 weeks old), and untreated old samples (again 109 weeks old). We evaluated four sources of DNA: blood ($n = 18$), liver ($n = 18$), heart ($n = 18$), and hypothalamus ($n = 18$).

Rats were euthanized at different ages by an overdose of isoflurane (> 5%).

The third batch of blood data was collected from both male ($n = 7$) and female ($n = 10$) Sprague-Dawley rats. Of these, $n = 9$ animals received E5, while $n = 8$ animals only received a saline injection (control). We collected two blood draws from each animal: at baseline (26 months old) and 2 weeks after treatment.

Trunk blood was collected immediately and stored at −80 °C until processing. A total of 100 µl blood sample was treated with 20 µl Proteinase K and then the volume was adjusted to 220 µl with phosphate buffer saline (PBS) in 1.5 ml or 2 ml microcentrifuge tube. A total of 200 µl buffer AL was mixed thoroughly to this mixture by vortexing, and incubated at 56 °C for 10 min. Then 200 µl ethanol (96–100%) was added to the sample and mix thoroughly by vortexing and DNA were extracted using the Qiagen DNeasy blood and tissue kit, Qiagen Cat No./ID: 69504 following manufacturer's instructions. The study protocol was approved through Institutional Animal Ethics Committee (approval no. CPCSEA/IAEC/P-6/2018) which was formed in accordance with the norms of the Committee for the Purpose of Control and Supervision of Experiments on Animals (CPCSEA), Government of India and complied with standard guidelines on handling of experimental animals.

Rats used in the glycan study

The rat samples for the IgG glycan aging measurement were from the above-mentioned mixed gender study but there is one notable difference: while the methylation study used samples extracted at day zero and just 15 days into the study, the glycan aging study used samples collected at day zero and at 168th day (15 days after 3rd dose). The date of day zero sample was June 17, 2022, while the date of the second time point/sample was December 2, 2022. We also used six young controls in the glycan aging study. Thus, we profiled serum

IgG N-glycome from six female treated, six female control, six male treated, six male control, and six young control. The older rats were all born between 17th and 19th April 2020. Young control rats were born between February and April 2022.

Human tissue samples

To build the human-rat clock, we analyzed previously generated methylation data from $n = 1366$ human tissue samples (adipose, blood, bone marrow, dermis, epidermis, heart, keratinocytes, fibroblasts, kidney, liver, lung, lymph node, muscle, pituitary, skin, spleen) from individuals whose ages ranged from 0 to 93. The data come from our study of primates [66]. Tissue and organ samples are from the National NeuroAIDS Tissue Consortium [67]. Blood samples are from the Cape Town Adolescent Antiretroviral Cohort study [68]. Skin and other primary cells provided by Raj et al. [57], Ethics approval (IRB#15-001454, IRB#16-000471, IRB#18-000315, IRB#16-002028).

Plasma fraction E5

The plasma fraction termed "E5" was developed by Harold Katcher and Akshay Sanghavi at Yuvan Research. This fraction was derived from the platelet-free plasma of young pigs (6–7 months old), an age at which pigs are typically slaughtered by farmers. The selection of this age, immediately post-puberty, is reflective of the mammalian youthful homeostatic peak, with the anticipation that this would be represented in the regulatory cargo circulating within the secretome [69]. This period marks the beginning of major aging-related changes globally [70]. The E5 treatment was formulated using plasma from pasture-fed, hormone-free tribal pigs (of the Yorkshire breed) in India. We have found it more complex to create E5 from porcine plasma obtained from pig farms in America.

To this platelet-free plasma, an equal volume of PEG solution in 0.5 Molar NaCl was added, and the combined mixture was incubated for 8 to 12 h at 4 °C. After the stipulated time, the solution was centrifuged at $1000 \times g$ for 5 min at 4 °C, and the supernatant was discarded. The sediment collected at the bottom of the tubes was transferred into a vessel and mixed with enough physiological saline buffer to make a suspension. The suspension obtained in the above step was subjected to size-exclusion chromatography. The fractions collected from size exclusion chromatography were recombined and concentrated. The concentrate was then mixed with sterile physiological saline solution and injected into rats through the tail vein.

In the following, we will provide more details on the treatment. Pig blood, sourced from pasture-raised pigs in India, was collected during slaughter via both the carotid artery and heart puncture. The collected blood was treated with acid citrate dextrose to prevent hemolysis and platelet activation, which we anticipated might dilute non-rejuvenating factors. We aimed to keep the blood temperature around 35 °C to avert platelet aggregation. Approximately 1.5 l of blood was procured per 60 kg animal.

The blood was subjected to centrifugation at room temperature (about 30 °C in Mumbai) at $500 \times g$ for 15 min. This allowed separation of the blood cells and platelet-rich plasma. Post-centrifugation, the plasma fraction was carefully collected using a pipet, ensuring no loss of larger ectosomes and exosomes. This plasma was further centrifuged at $2500 \times g$ for 25 min to pellet remaining platelets, and the supernatant platelet-poor plasma was stored at 4 °C.

Considering the requirement for large volumes of plasma, we employed a modified Extra-PEG method for exosome purification. This method involved an overnight precipitation of a plasma-PEG solution at 4 °C, followed by a low-speed centrifugation. Given the observed concentration dependency of nanoparticle numbers and protein-to-exosome ratios, we opted to use a final PEG concentration of 12%.

To eliminate protein aggregates and fibrin filaments, the redissolved PEG precipitate was passed through a Sephadex G100 column. The resulting fractions were pooled, concentrated via overnight dialysis, and stored appropriately depending on the intended use.

Experimental procedure

Although transfusion technologies for humans are well-developed and safe, transfusion of small animals is still at the infancy stage of development, requiring state-of-the-art techniques and remains challenging. The necessary dose of E5 was prepared and injected intravenously using sterile saline as vehicle.

Several assumptions underpinned the dosing for old rats (18 to 24 months old). These included estimations of blood mass as a percentage of body mass, the half-volume of plasma, the presence of pro-aging factors in old rat plasma, equivalence in concentration of anti-aging factors between young pig and rat blood, and preservation efficacy of the PEG process. Based on these assumptions, and in consideration of concentration dependency of exosome rejuvenation, the dosing was calculated such that the delivered pig anti-aging components would quadruple the concentration that would be present in young rat blood. This amounted to 1.43 g of solid precipitate per 500 g rat, administered as four injections every other day via tail veins.

The calculated doses were administered intravenously to the animals of old treated group; four injections every alternate day for 8 days, and a second dosing starting from the 95th day consisting of four injections every alternate day for 8 days, as shown in Supplementary Fig. 5. Similar amount of sterile saline solution (placebo) was administered to the animals of old control group. Body weight, food, and water intake of the animals were monitored at each time point. Cognitive abilities of animals were evaluated using Barnes maze apparatus (spanning a week of training) 1, 2, 3, and 4 months from the start of the 1st series of injections. Blood samples were withdrawn at predetermined time intervals by retro-orbital plexus during the treatment for hematological evaluation. Serum was separated from the blood samples of each animal and evaluated for biochemical parameters. Plasma was separated from the blood samples of each animal and was used for evaluation of inflammatory markers, i.e., TNF-α and IL-6. Animals were sacrificed from each group at 155th day of treatment and vital organs (brain, heart, lung, and liver) of these animals were harvested for testing of oxidative stress biomarkers, level of Nrf2, histopathological, and immunohistochemistry studies.

End-point evaluations

Body weight Body weights of rats were recorded before the initiation of treatment protocol and then 30, 60, 90, 120, and 155th day.

Grip strength A grip strength meter was used to measure forelimb grip strength which represents the muscle strength of animals. Briefly, as rat grasped the bar of muscle strength meter, the peak pull force was recorded on a digital force transducer. Tension was recorded at the time the rat released its forepaws from the bar. The grip strength in rats was measured using a grip strength meter, which records the peak pull force exerted by the rat in units of "grams" (g). Six consecutive measurements were taken per day at intervals of 1 min.

Barnes maze learning ability The Barnes maze platform (91 cm diameter, elevated 90 cm from the floor) consisted of 20 holes (each 5 cm in diameter). All holes were blocked except for one target hole that led to a recessed escape box. Spatial cues, bright light, and white noise were used to motivate the rat to find the escape during each session. For the adaptation phase, each rat explored the platform for 60 s. Any rat that did not find the escape box was guided to it and remained there for 90 s. For the acquisition phase, each trial followed the same protocol, with the goal to train each rat to find the target and enter the escape box within 180 s. Rat remained in the box for an additional 60 s. Four trials per day, approximately 15 min apart, was performed for six consecutive days. A Barnes maze apparatus used to determine the learning ability of the animals upon treatment. Performed in each month of experiment.

Hematological tests Blood was collected from the retro-orbital plexus using heparinized capillary tubes before the treatment and on 60th and 155th day of the experiment. One portion of the blood was kept in plain bottles from which serum was collected and stored for biochemical analysis. The other portion was directly subjected for the estimation of various hematological parameters using standard instruments. The levels of hemoglobin (Hb), red blood cell count (RBC), packed cell volume (PCV), MCV, MCH, MCHC, and platelets were analyzed in the blood samples in all experimental groups.

Biochemical test Blood samples were collected from the retro-orbital plexus using heparinized capillary tubes before the treatment and on 30th, 60th, 90th, 125th, and 155th day of the experiment. One portion of the blood was kept in plain bottles from which serum was collected and stored for biochemical analysis. Further, the levels of serum glutamate pyruvate transaminase (S.G.P.T.-IU/l) were carried out by kinetic method recommended by International Federation of Clinical Chemistry (IFCC). All the tests were performed with commercially available diagnostic kits (Erba Mannheim, Germany on Erba Mannheim biochemistry semi-autoanalyzer). Kidney function tests such as determination of serum creatinine (mg/dl) and uric acid (mg/dl) levels were done according to modified Jaffe's reaction with commercially available diagnostic kits (Erba Mannheim, Germany on Erba Mannheim biochemistry semi-autoanalyzer). Blood glucose level (random) (mg/dl) [71], total protein (g/dl), total bilirubin (mg/dl), direct bilirubin (mg/dl), triglyceride (mg/dl), HDL (mg/dl), cholesterol (mg/dl), and albumin (g/dl) (Erba Mannheim) were determined.

Potential impact of stress from blood collection on blood glucose levels

Laboratory animals, particularly rats, may undergo stress due to blood collection, which can inadvertently impact the study's results [72]. Such stressors can alter a range of physiological parameters including blood components, hormonal levels, wound healing rates, blood pressure, and heart rate. Notably, our rat subjects exhibited signs of stress, especially when blood was drawn from the suborbital plexus. The timing of the sample collection might have contributed to this stress since rats are nocturnal, and samples were taken during their typical rest period. We analyzed the influence of plasma fraction treatment on glucose levels at various intervals. Young rats showed slightly elevated blood glucose levels. Past studies have found that external stressors can increase glucose levels in rodents, yet levels below 199 are typically considered within a normal range [73, 74, 75]. In our observations, the glucose level ranging between 150 and 160 in the young control group is likely attributable to the stress experienced during sampling, rather than an indication of diabetes.

Oxidative stress evaluation At the end of experiment, brain, heart, lung, and liver were isolated and 10% tissue homogenate was prepared in ice-cold 50 mM PBS (pH 7.4) by using homogenizer followed by sonication for 5 min. The homogenate was centrifuged at 2000 g for 20 min at 4 °C and the aliquots of the supernatant were collected and stored at −20 °C up to further evaluation.

Estimation of extent of lipid peroxidation (LPO) (MDA) The brain, heart, lung, and liver tissue homogenate samples were treated with 1% phosphoric acid solution and aqueous solution of 0.6% thiobarbituric acid. The reaction mixture was heated at 80 °C for 45 min, cooled in an ice bath, and extracted with 4.0 ml of N-butanol. The n-butanol layer was separated, and the absorbance of the pink complex that formed was measured at 532 nm to indicate the extent of lipid peroxidation.

The n-butanol layer was separated using liquid-liquid extraction, commonly known as partitioning, with a separatory funnel. The mixture was added to the funnel and agitated until it settled into two distinct layers. The layers were then separated by opening the funnel's stopcock and draining the bottom layer, retaining the other layer inside the funnel.

Estimation of reduced GSH The GSH content in the brain, heart, lung, and liver tissue homogenate was determined by treating the homogenate with sulfhydryl reagent 5,5'-dithio-bis (2-nitrobenzoic acid) (DTNB) method. Briefly, 20 μl of tissue homogenate was treated with 180 μl of 1 mM DTNB solution at room temperature. The optical density of resulting yellow color was measured at 412 nm using a microplate spectrophotometer (Powerwave XS, Biotek, USA).

Determination of the catalase activity The brain, heart, lung, and liver tissue homogenate (20 μl) were added to 1 ml of 10 mM H_2O_2 solution in the quartz cuvette. The reduction in optical density of this mixture was measured by using spectrophotometer in UV mode at 240 nm. Rate of decrease in the optical density across 3 min from the addition of heart homogenate was taken as an indicator of the catalase activity present in the homogenate.

Estimation of SOD activity The brain, heart, lung, and liver tissue homogenates (20 μl) were added to a mixture of 20 μl of 500 mM of Na_2CO_3, 2 ml of 0.3% Triton X-100, 20 μl of 1.0 mM of EDTA, 5 ml of 10 mM of hydroxylamine, and 178 ml of distilled water. To this mixture, 20 μl of 240 μM of NBT was added. The optical density of this mixture was measured at 560 nm in kinetic mode for 3 min at 1-min intervals. The rate increase in the optical density was determined as indicator of the SOD activity.

Nrf2 concentration in vital organs   Nrf2 was estimated in brain, heart, lung, and liver homogenates using Nrf2 ELISA kit (Kinesis Dx, USA). Organ was removed and homogenate was prepared and kept at −20 °C until the execution of assay. The Nrf2 level was determined by using kit according to the manufacturer's protocol, and the values were calculated from the optical density of samples.

Pro-inflammatory cytokines (IL-6 and TNF-α)   The cytokines were estimated in plasma, which was separated from blood of animals and kept at −20 °C until the execution of assay. The pro-inflammatory cytokine levels including TNF-α and IL-6 were determined by using sandwich ELISA kit (Kinesis Dx, USA), according to the manufacturer's protocol, and the values were calculated from the optical density.

Histopathology of vital organs   Brain, heart, spleen, kidney, lung, liver, and testis tissues fixed in neutral buffered 10% formalin solution were embedded in paraffin, and serial sections (3 μm thick) were cut using microtome (Leica RM 2125, Germany). The representative sections were stained with hematoxylin and eosin and examined under light microscope (Leica, Germany). The histopathological sections were screened by a pathologist blinded to the treatments.

Oil red O staining   Cryosections (6 μm thick) were fixed in neutral buffered 10% formalin solution for 10 min. The slides were incubated with freshly prepared oil red O working solution for 15 min. Lipid accumulation was digitalized using a microscope.

DNA methylation profiling

For the first experimental series, we generated DNA methylation data using the mammalian methylation array "HorvathMammalMethylChip40" [38]. By design, the mammalian methylation array facilitates epigenetic studies across mammalian species (including rats and humans) due to its very high coverage (over thousand X) of highly conserved CpGs in mammals. These 36k CpGs exhibit flanking sequences that are highly conserved across mammals. The subset of species for each probe is provided in the chip manifest file which has been posted on Gene Expression Omnibus. The SeSaMe normalization method was used to define beta values for each probe [76].

For the second experimental series, we used the mammalian methylation 320 array platform to generate methylation data from blood. This array combines the CpG content of the mammal 40 array with the Illumina mouse array. The array contains 106K CpGs that map to the genome of the brown rat.

Unsupervised hierarchical clustering was performed to identify outliers and failed arrays, and those were excluded.

Penalized regression models

We developed the six different epigenetic clocks for rats by regressing chronological age on the CpGs on the mammalian array. We used all tissues for the pan-tissue clock. We restricted the analysis to blood, liver, and brain tissue for the blood, liver, and brain tissue clocks, respectively. Penalized regression models were created with the R function "glmnet" [77]. We investigated models produced by both "elastic net" regression (alpha = 0.5). The optimal penalty parameters in all cases were determined automatically by using a 10-fold internal cross-validation (cv.glmnet) on the training set. The alpha value for the elastic net regression was set to 0.5 (midpoint between Ridge and Lasso type regression) and was not optimized for model performance. We performed a cross-validation scheme for arriving at unbiased (or at least less biased) estimates of the accuracy of the different DNAm-based age estimators. One type consisted of leaving out a single sample (LOOCV) from the regression, predicting an age for that sample, and iterating over all samples.

Relative age estimation

To introduce biological meaning into age estimates of rats and humans that have very different lifespan, as well as to overcome the inevitable skewing due to unequal distribution of data points from rats and humans across age range, relative age estimation was made using the formula: Relative age = Age / maxLifespan where the maximum lifespan for rats and humans were set to 3.8 years and 122.5 years, respectively.

Epigenome-wide association studies of age and treatment

In our EWAS, we used the same data as those underlying Fig. 2 .

The normalized beta values were used to fit a least squares linear regression model using the R package limma (v3.50.0) [78]. The model was adjusted for known variables, including Condition, Sentrix_ID, and methylation array column. To account for unknown confounders, factor analysis was performed using the R package RUVSeq (v1.28.0) [79] and two RUVg vectors were added to the model. The defined model was used to identify differentially methylated cytosines in two distinct contrasts: (1) the age contrast, which aimed to detect differentially methylated loci associated with the aging process, and (2) the Elixir contrast, which compared treated rats with age-matched control rats to determine cytosines that exhibited differential methylation due to the treatment effect. Empirical Bayes statistics were estimated using the eBayes function, and multiple testing was using the Benjamini-Hochberg (BH) method. Probes with an adjusted p value < 0.05 were considered statistically significant.

The regression models for this study included the following covariates: SID, TreatmentCondition, Sentrix_ID, Col. The full model formula was: ~ 0 + TreatmentCondition + Sentrix_ID + Col. The null model formula was: ~ 0 + Sentrix_ID + Col.

Empirical Bayes correction was applied to model fits.

Limma's contrasts.fit function was used to perform group comparisons. Contrasts used:

Elixir = TreatmentConditionOldTreated − TreatmentConditionOldControl

Age = TreatmentConditionOldControl − TreatmentConditionYoungControl

For each data set and contrast, p values were adjusted with Benjamini-Hochberg correction for multiple testing and those with FDR $q <$ 0.05 were deemed significant.

Immunoaffinity enrichment of IgG from rat serum

Frozen serum samples were thawed at +4 °C, randomized, and 30 µl was transferred into a 96-well 1-ml collection plate. A total of seven standards prepared by pooling the samples as well as blanks were included to assess the technical variation and possible carryover and cross-contamination, respectively. The IgG was enriched on Pierce™ protein L agarose (Thermo Fisher Scientific Inc.) by downscaling our previously published protocol [80]. Briefly, the samples were diluted with 270 µl 1× PBS (pH 7.4), 20 µl of protein G beads were added, and the plate was sealed with an Easy Pierce heat sealing foil (Thermo Fisher Scientific Inc.) and shaken for 1 h on an orbital shaker (800 rpm). Next, the beads were transferred into a 1-ml PP filtration microplate (Agilent, 7 µm frit, cat. no. 202501-100) and washed 3× with 200 µl 1× PBS and 2× 200 µl ultrapure water. The IgG was eluted with 150 µl 0.1 M formic acid (Merck KGaA, Darmstadt) directly into a PCR plate containing 15 µl 1 M ammonium bicarbonate (Acros Organics, Geel, Belgium) solution by centrifugation (4 min, $60 \times g$). The eluate was dried down in a vacuum centrifuge at 40 °C.

Tryptic glycopeptide preparation and HILIC-SPE

Dry IgG was redissolved in 25 µl 25 mM ammonium bicarbonate and digested with 0.2 µg sequencing grade modified trypsin (Promega Corp., Madison WI, USA) at 37 °C overnight. Tryptic glycopeptides were enriched on Chromabond® zwitterionic HILIC adsorbent (Macherey-Nagel GmbH & Co., Düren, Germany) in a high-throughput manner, dried down in a vacuum centrifuge, and stored at −20 °C.

Nano-liquid chromatography-mass spectrometry and data pre-processing

The rat IgG-Fc N-glycosylation profiling was performed for IgG2a (P20760), IgG2b (P20761), and IgG2c (P20762) subclasses. Dry glycopeptides were redissolved in 30 µl ultrapure water and 5 µl was injected for analysis. The nano-LC-ESI-Q-TOF setup, chromatographic conditions, and MS parameters were thoroughly described in Habazin 2021 PMID: 34118474. MS1 files were first converted to mzXML format using ProteoWizard MSConvert (v. 3.0) and processed with LaCy Tools (v. 1.0.1), Chambers 2012 PMID: 23051804. Relative abundances of IgG N-glycoforms were calculated by normalizing the integrated areas of the extracted ion chromatograms to the total area for each of the three IgG subclasses.

Glycoproteomic data statistical analysis

Association analyses between chronological age and glycopeptide traits were performed using a general linear model with sex included as additional covariate. Longitudinal analysis of samples through their observation period was performed by implementing a linear mixed-effects model where time was modeled as a fixed effect, the interaction between time and plasma fraction treatment was modeled as a fixed effect, while individual sample ID was modeled as a random intercept. Prior to analyses, glycopeptide variables were all transformed to standard normal distribution (mean = 0, sd = 1) by inverse transformation of ranks to normality (R package "GenABEL," function rntransform). Using rank transformed variables in analyses makes estimated effects of different glycopeptides comparable as transformed glycopeptide variables have the same standardized variance. False discovery rate was controlled using Benjamini-Hochberg procedure. Data was analyzed and visualized using R programming language (version 4.0.2).

Publisher's note

Author contribution

The plasma fraction treatment was developed by Harold Katcher (HK) in consultation with Akshay Sanghavi (AS). KR, Steve Horvath (StH), and HK drafted the manuscript. All authors helped to edit the article. JZ and StH developed the epigenetic clocks. StH generated the DNA methylation data. JZ, KR, SK, CL, and StH carried out statistical analyses and created figures and tables. KS managed the plasma treatment project and carried out the experiments with SK and AgS. RG, HC, CH, LSW, MC-M, ML, PC, TW, and AM contributed rat tissue samples. AL and StH contributed human data. SiH, MN, FV, and GL carried out immunoglobulin G N-glycosylation analysis and analyzed the glycoproteomic data.

Declarations

Conflict of interest   Several authors are founders, owners, employees (Harold Katcher and Akshay Sanghavi), or consultants of Yuvan Research (Steve Horvath and Agnivesh Shrivastava) which plans to commercialize the E5 treatment. Other authors (Kavita Singh, Shraddha Khairnar) received financial support from Yuvan Research. Gordan Lauc is a founder and CEO of Genos Ltd., a company specialized in high-throughput glycomics. Siniša Habazin, Mislav Novokmet, and Frano Vučković are employees of Genos Ltd. The other authors do not have conflict of interest.

Supplementary information

ESM 1

(DOCX 20390 kb)

ESM 2

(CSV 1078 kb)

References

1. Conese M, Carbone A, Beccia E, Angiolillo A. The fountain of youth: a tale of parabiosis, stem cells, and rejuvenation. Open Med (Wars). 2017;12:376–83. https://doi.org/10.1515/med-2017-0053.

2. Mccay CM, Pope F, Lunsford W, Sperling G, Sambhavaphol P. Parabiosis between old and young rats. Gerontology. 1957;1:7–17.

3. Ludwig FC, Elashoff RM. Mortality in syngeneic rat parabionts of different chronological age. Trans N Y Acad Sci. 1972;34:582–7.

4. Eggel A, Wyss-Coray T. A revival of parabiosis in biomedical research. Swiss Med Wkly. 2014;144:w13914. https://doi.org/10.4414/smw.2014.13914.

5. Conboy MJ, Conboy IM, Rando TA. Heterochronic parabiosis: historical perspective and methodological considerations for studies of aging and longevity. Aging Cell. 2013;12:525–30.

6. Baht GS, et al. Exposure to a youthful circulation rejuvenates bone repair through modulation of β-catenin. Nat Commun. 2015;6:7131.

7. Conboy IM, et al. Rejuvenation of aged progenitor cells by exposure to a young systemic environment. Nature. 2005;433:760–4.

8. Huang Q, et al. A young blood environment decreases aging of senile mice kidneys. J Gerontol: Series A. 2018;73:421–8.

9. Katsimpardi L, et al. Vascular and neurogenic rejuvenation of the aging mouse brain by young systemic factors. Science. 2014;344:630–4.

10. Villeda SA, et al. The ageing systemic milieu negatively regulates neurogenesis and cognitive function. Nature. 2011;477:90–4.

11. Castellano JM, et al. Human umbilical cord plasma proteins revitalize hippocampal function in aged mice. Nature. 2017;544:488–92.

12. Villeda SA, et al. Young blood reverses age-related impairments in cognitive function and synaptic plasticity in mice. Nat Med. 2014;20:659–63. https://doi.org/10.1038/nm.3569.

13. Ferrucci L, et al. Measuring biological aging in humans: a quest. Aging Cell. 2020;19:e13080. https://doi.org/10.1111/acel.13080.

14. Sen P, Shah PP, Nativio R, Berger SL. Epigenetic mechanisms of longevity and aging. Cell. 2016;166:822–39. https://doi.org/10.1016/j.cell.2016.07.050.

15. Kane AE, Sinclair DA. Epigenetic changes during aging and their reprogramming potential. Crit Rev Biochem Mol Biol. 2019;54:61–83. https://doi.org/10.1080/10409238.2019.1570075.

16. Zhang W, Qu J, Liu G-H, Belmonte JCI. The ageing epigenome and its rejuvenation. Nat Rev Mol Cell Biol. 2020;21:137–50. https://doi.org/10.1038/s41580-019-0204-5.

17. Lopez-Otin C, Blasco MA, Partridge L, Serrano M, Kroemer G. The hallmarks of aging. Cell. 2013;153:1194–217. https://doi.org/10.1016/j.cell.2013.05.039.

18. Bocklandt S, et al. Epigenetic predictor of age. PloS One. 2011;6:e14821. https://doi.org/10.1371/journal.pone.0014821.

19. Garagnani P, et al. Methylation of ELOVL2 gene as a new epigenetic marker of age. Aging Cell. 2012;11:1132–4. https://doi.org/10.1111/acel.12005.

20. Horvath S. DNA methylation age of human tissues and cell types. Genome Biol. 2013;14:R115. https://doi.org/10.1186/gb-2013-14-10-r115.

21. Lin Q, et al. DNA methylation levels at individual age-associated CpG sites can be indicative for life expectancy. Aging (Albany NY). 2016;8:394–401.

22. Marioni R, et al. DNA methylation age of blood predicts all-cause mortality in later life. Genome Biol. 2015;16:25.

23. Chen BH, et al. DNA methylation-based measures of biological age: meta-analysis predicting time to death. Aging (Albany NY). 2016;8:1844–65. https://doi.org/10.18632/aging.101020.

24. Horvath S, et al. Decreased epigenetic age of PBMCs from Italian semi-supercentenarians and their offspring. Aging (Albany NY). 2015;7:1159–70. https://doi.org/10.18632/aging.100861.

25. Marioni RE, et al. The epigenetic clock is correlated with physical and cognitive fitness in the Lothian birth cohort 1936. Int J Epidemiol. 2015;44:1388–96. https://doi.org/10.1093/ije/dyu277.

26. Horvath S, et al. Accelerated epigenetic aging in Down syndrome. Aging Cell. 2015;14:491–5. https://doi.org/10.1111/acel.12325.

27. Dec E, et al. Centenarian clocks: epigenetic clocks for validating claims of exceptional longevity. Geroscience. 2023; https://doi.org/10.1007/s11357-023-00731-7.

28. Horvath S, Levine AJ. HIV-1 infection accelerates age according to the epigenetic clock. J Infect Dis. 2015;212:1563–73. https://doi.org/10.1093/infdis/jiv277.

29. Horvath S, et al. Obesity accelerates epigenetic aging of human liver. Proc Natl Acad Sci U S A. 2014;111:15538–43. https://doi.org/10.1073/pnas.1412759111.

30. Levine ME, et al. Menopause accelerates biological aging. Proc Natl Acad Sci U S A. 2016;113:9327–32. https://doi.org/10.1073/pnas.1604558113.

31. Petkovich DA, et al. Using DNA methylation profiling to evaluate biological age and longevity interventions. Cell Metab. 2017;25:954–960.e956. https://doi.org/10.1016/j.cmet.2017.03.016.

32. Cole JJ, et al. Diverse interventions that extend mouse lifespan suppress shared age-associated epigenetic changes at critical gene regulatory regions. Genome Biol. 2017;18:58. https://doi.org/10.1186/s13059-017-1185-3.

33. Wang T, et al. Epigenetic aging signatures in mice livers are slowed by dwarfism, calorie restriction and rapamycin treatment. Genome Biol. 2017;18:57. https://doi.org/10.1186/s13059-017-1186-2.

34. Thompson MJ, et al. A multi-tissue full lifespan epigenetic clock for mice. Aging (Albany NY). 2018;10:2832–54. https://doi.org/10.18632/aging.101590.

35. Meer MV, Podolskiy DI, Tyshkovskiy A, Gladyshev VN. A whole lifespan mouse multi-tissue DNA methylation clock. eLife. 2018;7:e40675. https://doi.org/10.7554/eLife.40675.

36. Mijakovac A, et al. Heritability of the glycan clock of biological age. Front Cell Dev Biol. 2022;10:982609. https://doi.org/10.3389/fcell.2022.982609.

37. Krištić J, Lauc G, Pezer M. Immunoglobulin G glycans — biomarkers and molecular effectors of aging. Clin Chim Acta. 2022;535:30–45. https://doi.org/10.1016/j.cca.2022.08.006.

38. Arneson A, et al. A mammalian methylation array for profiling methylation levels at conserved sequences. Nat Commun. 2022;13:783. https://doi.org/10.1038/s41467-022-28355-z.

39. Katcher HL. Studies that shed new light on aging. Biochemistry (Mosc). 2013;78:1061–70. https://doi.org/10.1134/s0006297913090137.

40. Rebo J, et al. A single heterochronic blood exchange reveals rapid inhibition of multiple tissues by old blood. Nat Commun. 2016;7:13363.

41. Ma Q. Role of nrf2 in oxidative stress and toxicity. Annu Rev Pharmacol Toxicol. 2013;53:401–26. https://doi.org/10.1146/annurev-pharmtox-011112-140320.

42. Nadon NL, Strong R, Miller RA, Harrison DE. NIA interventions testing program: investigating putative aging intervention agents in a genetically heterogeneous mouse model. EBioMedicine. 2017;21:3–4.

43. Chiavellini P, et al. Young plasma rejuvenates blood DNA methylation profile, prolongs mean lifespan and improves health in old rats. bioRxiv, 2022.2012.2001.518747. 2022; https://doi.org/10.1101/2022.12.01.518747.

44. Shkunnikova S, et al. IgG glycans in health and disease: prediction, intervention, prognosis, and therapy. Biotechnol Adv. 2023;67:108169. https://doi.org/10.1016/j.biotechadv.2023.108169.

45. Wang Y, et al. Exosomal circRNAs: biogenesis, effect and application in human diseases. Mol Cancer. 2019;18:116. https://doi.org/10.1186/s12943-019-1041-z.

46. Rider MA, Hurwitz SN, Meckes DG Jr. ExtraPEG: a polyethylene glycol-based method for enrichment of extracellular vesicles. Sci Rep. 2016;6:23978.

47. Andreu Z, Yáñez-Mó M. Tetraspanins in extracellular vesicle formation and function. Front Immunol. 2014;5:442. https://doi.org/10.3389/fimmu.2014.00442.

48. Horvath S, et al. Reversing age: dual species measurement of epigenetic age with a single clock. bioRxiv, 2020.2005.2007.082917. 2020; https://doi.org/10.1101/2020.05.07.082917.

49. Poganik JR, et al. Biological age is increased by stress and restored upon recovery. Cell Metab. 2023;35:807–820.e805. https://doi.org/10.1016/j.cmet.2023.03.015.

50. Zhang B, et al. Multi-omic rejuvenation and life span extension on exposure to youthful circulation. Nature Aging. 2023; https://doi.org/10.1038/s43587-023-00451-9.

51. Clement J, et al. Umbilical cord plasma concentrate has beneficial effects on DNA methylation GrimAge and human clinical biomarkers. Aging Cell. 2022;21:e13696. https://doi.org/10.1111/acel.13696.

52. Lu AT, et al. Universal DNA methylation age across mammalian tissues. Nature Aging. 2023; https://doi.org/10.1038/s43587-023-00462-6.

53. Lauc G, et al. Loci associated with N-glycosylation of human immunoglobulin G show pleiotropy with autoimmune diseases and haematological cancers. PLoS Genet. 2013;9:e1003225. https://doi.org/10.1371/journal.pgen.1003225.

54. Hanić M, et al. Anti-TNF biologicals enhance the anti-inflammatory properties of IgG N-glycome in Crohn's disease. Biomolecules. 2023;13 https://doi.org/10.3390/biom13060954.

55. Horvath S, et al. The cerebellum ages slowly according to the epigenetic clock. Aging (Albany NY). 2015;7:294–306.

56. Raj K, Horvath S. Current perspectives on the cellular and molecular features of epigenetic ageing. Exp Biol Med. 2020:1535370220918329. https://doi.org/10.1177/1535370220918329.

57. Kabacik S, Horvath S, Cohen H, Raj K. Epigenetic ageing is distinct from senescence-mediated ageing and is not prevented by telomerase expression. Aging (Albany NY). 2018;10:2800–15. https://doi.org/10.18632/aging.101588.

58. Lewis SK, et al. DNA methylation analysis validates organoids as a viable model for studying human intestinal aging. Cell Mol Gastroenterol Hepatol. 2020;9:527–41. https://doi.org/10.1016/j.jcmgh.2019.11.013.

59. Hernando-Herraez I, et al. Ageing affects DNA methylation drift and transcriptional cell-to-cell variability in mouse muscle stem cells. Nat Commun. 2019;10:4361. https://doi.org/10.1038/s41467-019-12293-4. http://europepmc.org/abstract/MED/31554804. https://europepmc.org/articles/PMC6761124. https://europepmc.org/articles/PMC6761124?pdf=render

60. Teschendorff AE, et al. Age-dependent DNA methylation of genes that are suppressed in stem cells is a hallmark of cancer. Genome Res. 2010;20:440–6. https://doi.org/10.1101/gr.103606.109.

61. Horvath S, Raj K. DNA methylation-based biomarkers and the epigenetic clock theory of ageing. Nat Rev Genet. 2018; https://doi.org/10.1038/s41576-018-0004-3.

62. Hoshino A, Horvath S, Sridhar A, Chitsazan A, Reh TA. Synchrony and asynchrony between an epigenetic clock and developmental timing. Sci Rep. 2019;9:3770. https://doi.org/10.1038/s41598-019-39919-3.

63. Yang J-H, et al. Loss of epigenetic information as a cause of mammalian aging. Cell. 2023;186:305–326.e327.

64. Stoeger T, et al. Aging is associated with a systemic length-associated transcriptome imbalance. Nature Aging. 2022;2:1191–206. https://doi.org/10.1038/s43587-022-00317-6.

65. Woods LC, Mott R. Heterogeneous stock populations for analysis of complex traits. Methods Mol Biol. 2017;1488:31–44. https://doi.org/10.1007/978-1-4939-6427-7_2.

66. Horvath S, et al. Pan-primate studies of age and sex. Geroscience. 2023; https://doi.org/10.1007/s11357-023-00878-3.

67. Morgello S, et al. The National NeuroAIDS Tissue Consortium: a new paradigm in brain banking with an emphasis on infectious disease. Neuropathol Appl Neurobiol. 2001;27:326–35.

68. Horvath S, et al. Perinatally acquired HIV infection accelerates epigenetic aging in South African adolescents. AIDS. 2018;32:1465–74. https://doi.org/10.1097/QAD.0000000000001854.

69. Reiland S. Growth and skeletal development of the pig. Acta Radiol Suppl. 1978;358:15–22.

70. Labbadia J, Morimoto RI. Repression of the heat shock response is a programmed event at the onset of reproduction. Mol Cell. 2015;59:639–50. https://doi.org/10.1016/j.molcel.2015.06.027.

71. Gaikwad SM, Mulay P, Joshi RR. Analytical hierarchy process to recommend an ice cream to a diabetic patient based on sugar content in it. Procedia Computer Science. 2015;50:64–72.

72. Nowland MH, Hugunin K, Rogers KL. Effects of short-term fasting in male Sprague–Dawley rats. Comp Med. 2011;61:138–44.

73. Clee SM, Attie AD. The genetic landscape of type 2 diabetes in mice. Endocr Rev. 2007;28:48–83.

74. Svenson KL, et al. Multiple trait measurements in 43 inbred mouse strains capture the phenotypic diversity characteristic of human populations. J Appl Physiol. 2007;102:2369–78.

75. Fajardo RJ, Karim L, Calley VI, Bouxsein ML. A review of rodent models of type 2 diabetic skeletal fragility. J Bone Miner Res. 2014;29:1025–40.

76. Zhou W, Triche TJ Jr, Laird PW, Shen H. SeSAMe: reducing artifactual detection of DNA methylation by Infinium BeadChips in genomic deletions. Nucleic Acids Res. 2018;46:e123. https://doi.org/10.1093/nar/gky691.

77. Friedman J, Hastie T, Tibshirani R. Regularization paths for generalized linear models via coordinate descent. J Stat Softw. 2010;33:1–22.

78. Ritchie ME, et al. limma powers differential expression analyses for RNA-sequencing and microarray studies. Nucleic Acids Res. 2015;43:e47. https://doi.org/10.1093/nar/gkv007.

79. Risso D, Ngai J, Speed TP, Dudoit S. Normalization of RNA-seq data using factor analysis of control genes or samples. Nat Biotechnol. 2014;32:896–902. https://doi.org/10.1038/nbt.2931.

80. Habazin S, et al. High-throughput rat immunoglobulin G N-glycosylation profiling revealed subclass-specific changes associated with chronic stress. J Proteomics. 2021;245:104293. https://doi.org/10.1016/j.jprot.2021.104293.